Title
An ozone episode in the Pearl River Delta: Field observation and model simulation

Journal
Journal of Geophysical Research, 115(D22)

ISSN
0148-0227

Authors
Jiang, F
Guo, H
Wang, TJ
et al.

Publication Date
2010

DOI
10.1029/2009jd013583

An ozone episode in the Pearl River Delta: Field observation and model simulation

F. Jiang,[1,2] H. Guo,[1] T. J. Wang,[2] H. R. Cheng,[1] X. M. Wang,[3] I. J. Simpson,[4] A. J. Ding,[2] S. M. Saunders,[5] S. H. M. Lam,[5] and D. R. Blake[4]

Received 20 November 2009; revised 19 July 2010; accepted 10 August 2010; published 23 November 2010.

[1] In the fall of 2007 concurrent air sampling field measurements were conducted for the first time in Guangzhou (at Wan Qing Sha (WQS)) and Hong Kong (at Tung Chung (TC)), two cities in the rapidly developing Pearl River Delta region of China that are only 62 km apart. This region is known to suffer from poor air quality, especially during the autumn and winter months, when the prevailing meteorological conditions bring an outflow of continental air to the region. An interesting multiday O_3 pollution event (daily maximum O_3 > 122 ppbv) was captured during 9–17 November at WQS, while only one O_3 episode day (10 November) was observed at TC during this time. The mean O_3 mixing ratios at TC and WQS during the episode were 38 ± 3 (mean ± 95% confidence interval) and 51 ± 7 ppbv, respectively, with a mean difference of 13 ppbv and a maximum hourly difference of 150 ppbv. We further divided this event into two periods: 9–11 November as Period 1 and 12–17 November as Period 2. The mixing ratios of O_3 and its precursors (NO_x and CO) showed significant differences between the two periods at TC. By contrast, no obvious difference was found at WQS, indicating that different air masses arrived at TC for the two periods, as opposed to similar air masses at WQS for both periods. The analysis of VOC ratios and their relationship with O_3 revealed strong O_3 production at WQS during Period 2, in contrast to relatively weak photochemical O_3 formation at TC. The weather conditions implied regional transport of O_3 pollution during Period 1 at both sites. Furthermore, a comprehensive air quality model system (Weather Research and Forecasting–Community Multiscale Air Quality model (WRF-CMAQ)) was used to simulate this O_3 pollution event. The model system generally reproduced the variations of weather conditions, simulated well the continuous high O_3 episode event at WQS, and captured fairly well the elevated O_3 mixing ratios in Period 1 and low O_3 levels in Period 2 at TC. The modeled surface O_3 distributions and flow structures clearly illustrated the occurrence of O_3 formation and the impact of regional transport on O_3 levels in Period 1 in the Pearl River Delta. Further analysis of O_3 formation indicated that horizontal transport was the main contributor to the O_3 increase at TC during Period 1, while at WQS O_3 levels were dominated by photochemical production during both periods. The low O_3 levels at TC during Period 2 were attributable to lower temperatures and the arrival of fresh maritime air masses brought in by strong easterly winds. This study highlights how contrasting precursor concentrations and photochemical conditions can occur over a very small distance, and it provides a rare opportunity to better understand ozone production and precursor source origins on a finer scale in this region.

Citation: Jiang, F., H. Guo, T. J. Wang, H. R. Cheng, X. M. Wang, I. J. Simpson, A. J. Ding, S. M. Saunders, S. H. M. Lam, and D. R. Blake (2010), An ozone episode in the Pearl River Delta: Field observation and model simulation, *J. Geophys. Res.*, *115*, D22305, doi:10.1029/2009JD013583.

[1]Air Quality Studies, Department of Civil and Structural Engineering, Hong Kong Polytechnic University, Hong Kong.
[2]School of Atmospheric Sciences, Nanjing University, Nanjing, China.
[3]Guangzhou Institute of Geochemistry, Chinese Academy of Sciences, Guangzhou, China.
[4]Department of Chemistry, University of California at Irvine, California, USA.
[5]School of Biomedical, Biomolecular, and Chemical Sciences, University of Western Australia, Perth, Australia.

0148-0227/10/2009JD013583

1. Introduction

[2] Photochemical ozone (O_3) pollution has become one of the major air pollution problems in the Pearl River Delta (PRD) region of southern China [e.g., *Wang et al.*, 1998; *Streets et al.*, 2006; *Zhang et al.*, 2008a; *Guo et al.*, 2009]. The PRD region consists of nine cities in mainland China (called the inland PRD), Hong Kong, and Macau. With the rapid economic growth in the region, emissions of major air pollutants have significantly increased since the early 1980s. For instance, the average ambient level of NO_x ($NO + NO_2$), one of the most important O_3 precursors, increased from 56 μg m^{-3} in 1991 to 70 μg m^{-3} in 1996 in the region [*Shao et al.*, 2009]. Consequently, photochemical O_3 pollution has become more and more serious in recent years. Indeed, a 14-year continuous study provides clear evidence that O_3 levels in the background atmosphere of Southern China have exhibited a slow rising trend since 1994 [*Wang et al.*, 2009].

[3] Photochemical O_3 pollution has been studied in South China for more than a decade. *Lam et al.* [1996] analyzed the behavior of background surface O_3 measured at a coastal site in Hong Kong, and *Chan et al.* [1998] compared background and urban O_3 levels in Hong Kong. They focused on seasonal variation of O_3 and related the observed trend to the large-scale Asian monsoon circulation. Low O_3 levels during summer were attributed to the inflow of maritime air, and abundant O_3 in autumn and winter was due to ample sunshine hours plus the outflow of O_3 precursor–laden continental air from the northeast or north. By analyzing a multiday photochemical smog episode in September 2001, *Wang and Kwok* [2003] found the contribution of regional emissions to the high O_3 in western Hong Kong. *Wang et al.* [2006] found evidence that regional transport played an important role in the formation of an O_3 episode observed on 27–31 March 2000, in Hong Kong. *Huang et al.* [2006] investigated 54 O_3 episodes that occurred over Hong Kong in 2000–2004 and found that 78% of these episodes were dominated by regional transport. In addition to such episodes in Hong Kong, photochemical O_3 pollution episodes have been observed frequently in Guangzhou and its suburbs, with hourly mixing ratios often exceeding 100 ppbv since early 1995 [*Zhang et al.*, 1999, 2008a; *Zheng et al.*, 2010]. *Zhang et al.* [2008a] conducted extensive field measurements of major air pollutants in the inland PRD region (exclusive of Hong Kong and Macau). High levels of O_3 exceeding China's national standard (hourly standard 75 ppbv) and evidence of regional-scale photochemical production of O_3 were often observed in their studies. Recently, *Zheng et al.* [2010] analyzed data from a regional air quality monitoring network and concluded that O_3 pollution in the PRD region exhibited both regional and superregional characteristics.

[4] Apart from regional transport, local chemical production is another factor in the high O_3 levels observed in the PRD. *So and Wang* [2003] reported that the O_3 variability at the southwestern suburban and urban sites in Hong Kong was more influenced by local emissions. *Huang et al.* [2006] found that 22% of the 54 O_3 episodes observed in 2000–2004 were due to local photochemical formation. *Jiang et al.* [2008] simulated a continuous photochemical pollution episode in September 2001 in Hong Kong and indicated the importance of local production of O_3. *Wang et al.* [2006] found that clear skies with high temperature and low humidity (caused by the strong high-pressure system over South China), as well as local emissions, were the cause of the high O_3 levels observed in March 2000.

[5] Sea-land breezes play an important role in transporting air pollution from urban areas to the coast. *Wang et al.* [1998] found that the local-scale recirculation was an important mechanism in transporting O_3 to the Hok Tsui monitoring site on Hong Kong Island. *Ding et al.* [2004] simulated the sea-land breezes associated with a multiday episode in the PRD region. They believed that the offshore synoptic wind, the delayed sea breezes, and the low mixing height contributed to the daytime transport of pollution and high O_3 on the coast. *Wang and Kwok* [2003] found that air pollutant concentrations during a smog episode in the PRD were closely related to the sea-land breezes. Recently, *Wang et al.* [2010] indicated that sea-land circulation played an important role in regional O_3 formation and distribution over the PRD. More than 75% of days featured interactions between weak synoptic forcing and local sea-land circulation in October 2004.

[6] Though many studies of O_3 have been conducted in the PRD, including Hong Kong, a detailed understanding of the mechanism of O_3 formation and distribution in the region is still a long-term scientific issue. One of the main reasons limiting progress in this area is the lack of concurrent field measurement data in the inland PRD and in Hong Kong that could link O_3 pollution in these regions and lead to a better understanding of photochemical smog. Hence, simultaneous measurements of O_3 and its precursors (i.e., VOCs and NO_x) in these two areas were conducted in October–December 2007. An overview of the project was given by *Guo et al.* [2009]. The relationship between O_3 and its precursors was simulated by using an observation-based model [*Cheng et al.*, 2010]. This paper will mainly focus on an O_3 episode event observed during the sampling period that provides a rare chance to understand the interaction of O_3 pollution between the inland PRD and Hong Kong. A model system (i.e., the Weather Research and Forecasting–Community Multiscale Air Quality model (WRF-CMAQ)) was used to simulate this episode event. The model performances of the simulation of wind fields and air pollution are discussed in detail, and the distribution of surface O_3 and the wind structure during the episode event are presented. The physical and chemical processes of the atmosphere are also quantitatively investigated to understand the different contributions of horizontal transport and photochemical reaction to O_3 formation in Hong Kong and the inland PRD region during the episode event.

2. Methodology

2.1. Field Measurements

[7] Air pollution data were simultaneously collected at two sites, namely Wan Qing Sha (WQS) and Tung Chung (TC), which are located in Guangzhou and Hong Kong, respectively (Figure 1). Detailed descriptions of the sites can be found in *Guo et al.* [2009]. The field measurements were carried out from 23 October to 1 December 2007. Trace gases, including O_3, NO-NO_2-NO_x, CO, and SO_2, were continuously sampled at WQS. Ozone was measured using a commercial UV photometric analyzer (Thermo Environmental Instruments (TEI), model 49C); SO_2 was measured by a pulsed UV fluorescence (TEI, model 43S); NO and

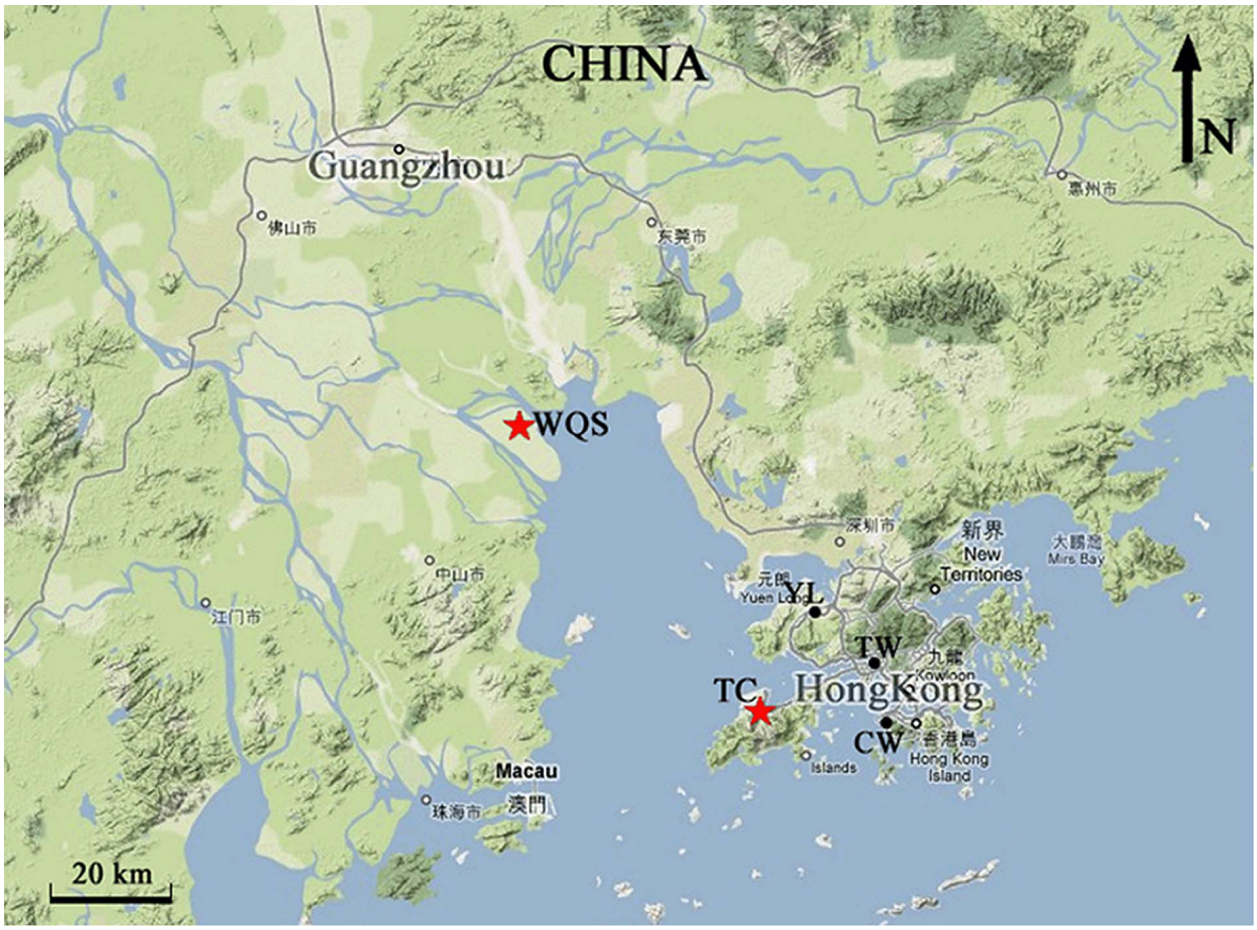

Figure 1. Location of the air monitoring sites.

NO_x were detected using a chemiluminescence NO-NO_2-NO_x analyzer (Thermo Electron Corporation, Model 42*i* trace level), and CO was measured with a gas filter correlation, nondispersive infrared analyzer (API, Model 300). The detection limits of O_3, SO_2, and NO-NO_2-NO_x were 2 ppbv, 0.06 ppbv, and 0.05 ppbv, respectively. The hourly data of O_3, CO, SO_2, and NO_x at the TC site were obtained from the web site of the Hong Kong Environmental Protection Department (HKEPD, http://www.epd.gov.hk). During the sampling period, ambient nonmethane hydrocarbon (NMHC) samples were collected using cleaned and evacuated 2 L electropolished stainless steel canisters on selected days (26–27 October; 13, 15–17, 23 November; and 1 December) at both sites. On these days, hourly NMHC samples were collected from 0700 to 1800 LST (local standard time) at TC, and from 0600 to 1800 LST at WQS. The samples were analyzed by an Entech Model 7100 Preconcentrator (Entech Instruments Inc., California, USA) coupled with a gas chromatography–mass selective detector (GC-MSD, Agilent 5973N). The MSD was used in selected ion monitoring (SIM) mode and the ionization method was electron impacting (EI). The detection limit of aromatics is 0.003 ppbv, and that of other NMHCs is 0.005 ppbv. The precision of the NMHC measurements varied compound by compound and ranged from 0.5% for ethane to 34% for *trans*-2-butene. Carbonyl samples were collected simultaneously at both sites on the same selected days. Samples were collected at 0.4–0.5 L min^{-1} for 150 min using a carbonyl sampler (Moore Products Co., USA), and about four carbonyl samples were collected during each sampling day. Typically C1–C8 carbonyl compounds were measured by high-performance liquid chromatography (HPLC) which has a detection limit of ~0.2 ppbv. Detailed descriptions of the measurement techniques and the quality control and assurance for trace gases, NMHCs, and carbonyls can be found in *Guo et al.* [2009]. In this study, additional hourly O_3 data from urban Hong Kong air quality monitoring stations were used for further analysis. The selected stations are Central/Western (CW), Tsuen Wan (TW), and Yuen Long (YL) (Figure 1). The CW and TW stations are in the urban center of Hong Kong, while the YL station is in the northwest of Hong Kong. More information on these sites can be found in a Hong Kong Environmental Protection Department (HKEPD) report [*HKEPD*, 2007].

2.2. Model Description and Configurations

2.2.1. Model Description and Meteorological Data

[8] The U.S. Environmental Protection Agency's Community Multiscale Air Quality (CMAQ) model was used to simulate the O_3 concentrations during the episode period. CMAQ is a three-dimensional Eulerian atmospheric chemistry and transport modeling system. It is designed as a one-atmosphere model, which can treat multiple pollutants simultaneously from local to continental scales and includes complex physics and chemical processes, such as gas and

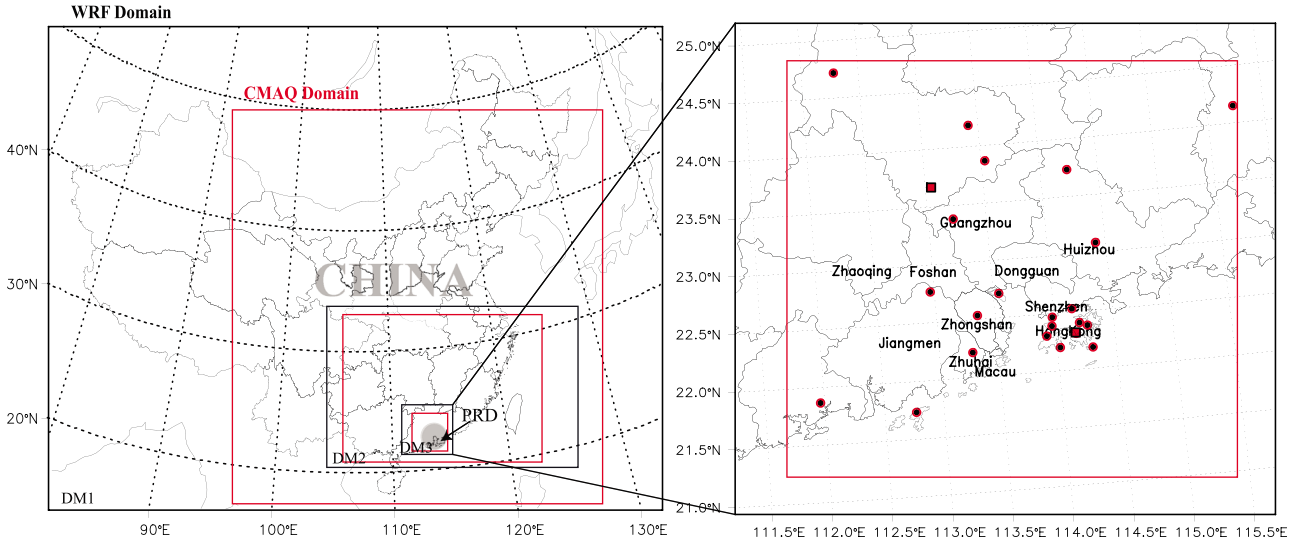

Figure 2. Nested domains of WRF and CMAQ modeling (black frames: WRF modeling domains, red frames: CMAQ modeling domains, circles: surface meteorological sites, squares: sounding stations).

aqueous chemical transformation, aerosol chemistry and dynamics, deposition, and photolysis. In this study, CMAQ was driven by the Weather Research and Forecasting (WRF) model [*Skamarock et al.*, 2008] (available at http://www.mmm.ucar.edu/wrf/users/docs/arw_v3.pdf). The WRF model is a next-generation mesoscale numerical weather prediction system designed to serve both operational forecasting and atmospheric research needs. It is suitable for use in a broad spectrum of applications across scales ranging from meters to thousands of kilometers, and it has been demonstrated to have good performance in all kinds of weather forecasts.

[9] Meteorological data from 22 surface weather stations (including WQS and TC) and 2 sounding stations were used in this modeling study. The meteorological data at WQS were simultaneously measured using a miniature weather station (Vantage Pro2, Davis Instruments Corp., USA), while data at TC were provided by the HKEPD. Except for TC and WQS, the surface data in Hong Kong were obtained from the Hong Kong Observatory, while data at the surface stations in the inner PRD region were provided by the State Meteorological Administration of China. The meteorological data in Hong Kong and at WQS have a time interval of 1 h, while the other surface data were generally in time intervals of 3 h.

2.2.2. Model Configurations

[10] In the WRF modeling, the simulation period was conducted from 0000 UTC 07 November to 0000 UTC 18 November 2007. Three nested domains were defined, with horizontal grids of 81 × 61, 97 × 61, and 61 × 61, respectively (Figure 2). The corresponding grid spacings are 75 km, 27 km, and 8.3 km. The outermost domain (DM1, 75 km) covers the whole China continental region, and the finest domain (DM3, 8.3 km) focuses on the PRD region. Vertically, there are 31 sigma levels, with the top pressure fixed at 100 hPa. These grid systems have been successfully used in a previous O_3 episode study by *Jiang et al.* [2008]. In addition, the physical parameterization configurations are also consistent with those in *Jiang et al.*. In this study, two approaches have been used to improve the model performance. First, four-dimensional data assimilation (FDDA), including grid analysis nudging and observational nudging, was applied; this continuous dynamical assimilation could reduce the model uncertainties and thereby increase the modeling accuracy. The effects of FDDA on the simulated meteorological fields and predicted O_3 concentrations have been investigated in previous studies [e.g., *Barna and Lamb*, 2000; *Choi et al.*, 2009]. Grid analysis nudging using the National Center for Environmental Protection (NCEP) 1° × 1° reanalysis data was applied on the outermost domain [*Stauffer and Seaman*, 1990], while observational nudging was applied in the finest domain [*Liu et al.*, 2005]. Meteorological data from 22 surface weather stations and 2 sounding stations in the PRD region were assimilated into the WRF simulation (site locations shown in Figure 2). Second, a single-layer urban canopy model was adopted in this study [*Kusaka and Kimura*, 2004], and the urban land-use data of the PRD region from the 2001 MODIS land cover product (http://webmap.ornl.gov/wcsdown/) was aggregated to the finest domain to replace the default U.S. Geological Survey (USGS) data in the WRF model. This substitution was made because the default USGS data are based on Advanced Very High Resolution Radiometer (AVHRR) observations from 1992–1993, making them too old to be representative of the PRD region today, especially because the land-use change in the PRD region has been found to have a significant influence on the predicted meteorological conditions and surface O_3 distribution [*X. M. Wang et al.*, 2007].

[11] The nesting technique was also used in the CMAQ simulation. As in the WRF modeling, three domains were defined with a grid spacing the same as the corresponding WRF domain, but with horizontal grids smaller than the WRF domain (see Figure 2). There are 16 layers in the CMAQ vertical coordinate, with the lowest 10 layers coinciding with those of WRF. In CMAQ chemical modeling, the gas-phase atmospheric chemistry is based on the SAPRC-99 mechanism [*Carter*, 2000] (available at http://www.cert.ucr.edu/~carter/pubs/), which considers 74 species and 211

reactions, and the aerosol chemistry and dynamics is simulated by the AERO3 aerosol module [*Binkowski*, 1999]. The process analysis module can track the quantitative effects of individual chemical and physical processes contributing to the concentrations of chemical species [*Gipson*, 1999]. In this study, the process analysis module was used to provide quantitative information about the impact of each process on the simulated hourly O_3 concentrations.

[12] Anthropogenic emission data were obtained from *Zhang et al.* [2009], which is the latest emission inventory in Asia (for the year 2006) developed to support the NASA Intercontinental Chemical Transport Experiment Phase B (INTEX-B) program. These inventories were compiled considering all major anthropogenic sources but excluding biomass burning. The biogenic emissions were calculated by using the Model of Emissions of Gases and Aerosols from Nature (MEGAN), version 2.04 [*Guenther et al.*, 2006]. MEGAN is a global biogenic emission model, and it is designed for both global and regional emission modeling and has global coverage with about 1 km^2 spatial resolution.

3. Results and Discussion

3.1. Characteristics of Air Pollutants During the Episode Event

3.1.1. Temporal Variation of O_3 Mixing Ratios

[13] A very interesting O_3 episode event was captured in the PRD region during 9–17 November 2007 (Figure 3). The event, in which the daily O_3 peak consistently exceeded the Hong Kong Air Quality Objective of 122 ppbv (one-hour standard) and China's National Standard of 75 ppbv (one-hour standard), lasted 8 days at the inland PRD site (i.e., WQS), with a peak O_3 mixing ratio of 182 ppbv, but only 1 day at the Hong Kong site (i.e., TC), with a peak value of 124 ppbv. Such a phenomenon is not an isolated case in the region. By analyzing the data obtained from the PRD Regional Air Quality Monitoring Network (http://www.epd.gov.hk/epd/english/resources_pub/publications/m_report.html) and the literature [*Zheng et al.*, 2010], 11 and 16 similar cases were identified in 2006 and 2007, respectively. Most of them occurred in warm months (i.e., May–November). One case identified in 2006 occurred at exactly the same time of year as this study (i.e., 9–17 November 2007). On 8–10 November 2006, the maximum hourly O_3 level at WQS reached 172, 121, and 156 ppb, respectively, while the highest O_3 mixing ratio was 66, 58, and 69 ppb, respectively. In the present study, the O_3 mixing ratio at both sites began to rise on 9 November and exceeded 122 ppbv on 10 November. Then the O_3 level at TC began to decrease and remained around 40 ppbv from 12 to 17 November. However, the O_3 mixing ratio at WQS continued to increase, with a daily maximum value higher than 150 ppbv from 12 to 17 November. It is noteworthy that the nighttime O_3 mixing ratios at TC were higher than those measured at WQS, a difference probably attributable to the constant transport of O_3 to TC by southeasterly flows from the South China Sea, where O_3 was consumed less [*Guo et al.*, 2009]. During 9–17 November, the mean O_3 mixing ratios at TC and WQS were 38 ± 3 (mean ± 95% confidence interval, same hereafter) and 51 ± 7 ppbv, respectively. The difference of the mean O_3 levels between the two sites during the event was 13 ppbv, but sometimes the hourly differences reached 150 ppbv. In addition, the spatiotemporal pattern of "oxidant" O_x ($O_3 + NO_2$), which is considered to be a better representation of O_3 levels as it takes into account the effect of O_3 titration by NO [*Jenkin*, 2004], is also shown in Figure 3. It can be seen that the temporal and spatial characteristics of $O_3 + NO_2$ mixing ratios were similar to those of O_3 alone. For completeness, the time series of NO and NO_2 mixing ratios are given in Figure 3 as well. Since the two sites are separated by a distance of only about 62 km, what would be the causes for such a huge discrepancy of O_3 levels observed between Hong Kong and the inland PRD region during the episode event?

[14] To gain further information on the O_3 episode event in Hong Kong, we examined air monitoring data at other Hong Kong ambient air monitoring stations. Figure 4 shows the hourly O_3 mixing ratios measured at four sites in Hong Kong (including TC). During 9–11 November, elevated O_3 mixing ratios were found at all four sites, and the O_3 peaks at the Yuen Long (YL) site were similar to those at the TC site. However, the maximum O_3 levels at the urban center stations, i.e., Central/Western (CW, 65 ppbv) and Tsuen Wan (TW, 59 ppbv) were much lower than those at YL (104 ppbv) and TC (124 ppbv), likely because of the titration of O_3 by very fresh emissions of NO from vehicles in the urban center. The similar temporal patterns of O_3 at the four Hong Kong sites and the WQS site suggest that O_3 pollution episodes from 9–11 November were indeed regional. It is noteworthy that the O_3 peaks at TC lagged those at YL. Since YL is much closer to the inland PRD region (7 km, compared to 26 km for TC), the lagged peaks at TC further implied that there might be regional transport of O_3 from the inland PRD region. On the other hand, during 12–17 November, the O_3 mixing ratios at the four Hong Kong sites generally remained at a low level of about 40 ppbv, suggesting that the photochemical O_3 formation was relatively weak over the Hong Kong area during that time.

3.1.2. Levels of Ozone Precursors

[15] On the basis of the variation of O_3 levels at the Hong Kong sites, we divided this event into two periods: Period 1, 9–11 November; and Period 2, 12–17 November (Figure 4). Table 1 shows the mean and median mixing ratios of O_3 and its precursors (i.e., NO_x, CO, NMHCs) during the daytime (i.e., 0600–1800 LST) for the two periods. The mean mixing ratio of O_3 at TC for Period 1 (48 ± 10 ppbv) was significantly greater than that for Period 2 (34 ± 2 ppbv) ($p < 0.01$). However, no significant difference in O_3 levels was found at WQS between the two periods ($p = 0.3$) (Table 1). By inspecting the O_3 precursors, we found that both NO_x and CO levels at TC were significantly different between the two periods ($p < 0.001$). That is, at the TC site, the NO_x and CO mixing ratios were much higher in Period 1 (56 ± 6 and 519 ± 33 ppbv, respectively) than in Period 2 (39 ± 4 and 354 ± 13 ppbv, respectively), which is consistent with the observation that O_3 levels at TC were much higher during Period 1 compared to Period 2. Since no VOC samples were taken in Period 1, the levels of total NMHCs could not be compared between the two periods. The mean mixing ratio of total NMHCs at TC for Period 2 was 30 ppbv, similar to the mean value for the entire sampling period (26 ± 3 ppbv, *Guo et al.*, 2009). In contrast, at WQS no significant difference in NO_x (32 ± 6 vs. 38 ± 5 ppbv)

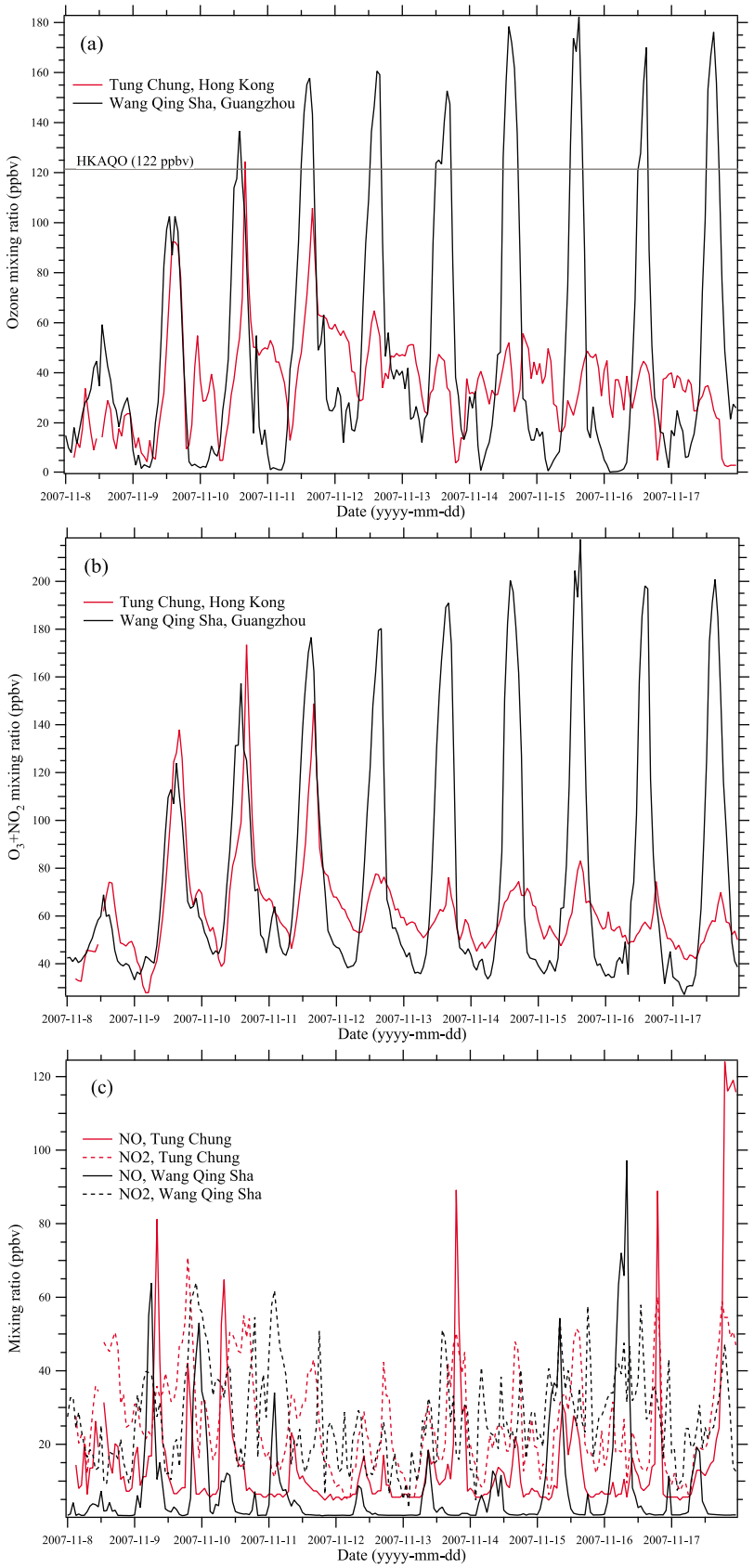

Figure 3. (a) Hourly ozone mixing ratios, (b) ozone plus NO_2 mixing ratios, and (c) NO and NO_2 mixing ratios at the TC and WQS sites between 0000 LST 8 November and 2300 LST 17 November 2007.

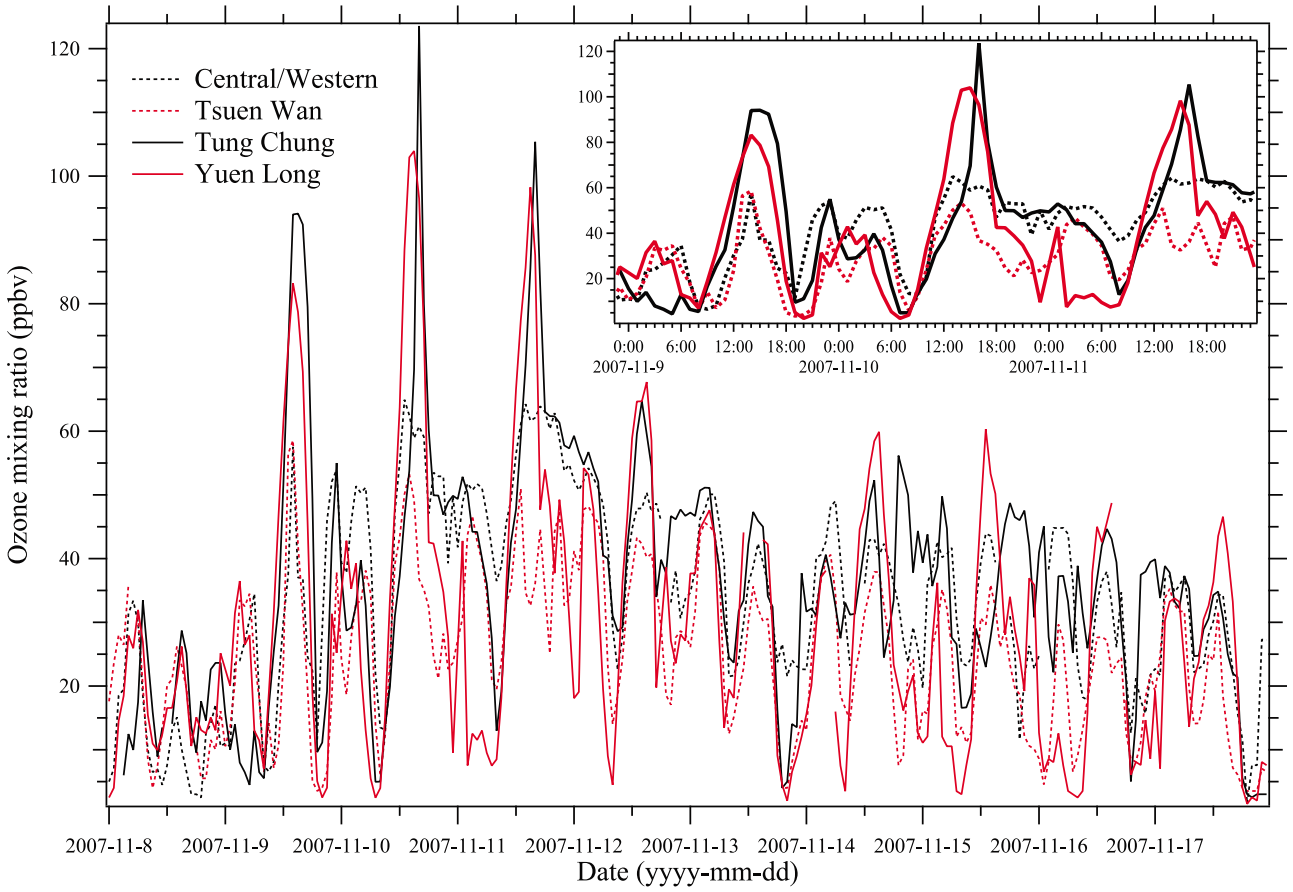

Figure 4. Hourly ozone mixing ratios at TC and three other air monitoring stations in urban Hong Kong.

and CO (1262 ± 98 vs. 1123 ± 71 ppbv) mixing ratios was found between the two periods ($P > 0.12$). These values are consistent with those for the whole sampling period (31 ± 2 ppbv for NO_x and 1047 ± 38 ppbv for CO, *Guo et al.*, 2009). In addition, the average level of total NMHCs (52 ppbv) in Period 2 was within 25% of that from the entire sampling period (39 ± 6 ppbv) [*Guo et al.*, 2009]. It is noteworthy that Period 2 at TC was the only sector with low O_3 levels. The lower mean O_3 mixing ratio (34 ± 2 ppbv) at TC corresponded to mean CO (354 ± 13 ppbv) and total NMHCs (30 ± 4 ppbv) levels that were lower than those at WQS during Period 2 (see Table 2). However, there was no difference in the mean NO_x mixing ratios between TC and WQS in Period 2, suggesting that CO and total NMHCs play key roles in O_3 formation at these two sites. Indeed, studies have found that O_3 production throughout much of the Hong Kong area (including the TC site) and in the central inland PRD and surrounding coastal areas (including the WQS site) is VOC limited [*Zhang et al.*, 2007; *Zhang et al.*, 2008b; *Cheng et al.*, 2010; *Wang et al.*, 2010].

Table 1. Mean Mixing Ratios of O_3 and Its Precursors During the Daytime Hours (0600–1800 LST) of the Two Periods

Species	Site	Period 1[a]		Period 2[b]	
		Mean ± 95%CI[c]	Median	Mean ± 95%CI	Median
O_3 (ppbv)	TC	48 ± 10	47	34 ± 2	33
	WQS	73 ± 14	73	83 ± 13	80
$O_3 + NO_2$ (ppbv)	TC	86 ± 11	85	60 ± 2	58
	WQS	98 ± 12	100	112 ± 13	110
NO_x (ppbv)	TC	56 ± 6	54	39 ± 4	34
	WQS	32 ± 6	26	38 ± 5	33
CO (ppbv)	TC	519 ± 33	537	354 ± 13	351
	WQS	1262 ± 98	1182	1123 ± 71	1041
Total NMHCs (ppbv)	TC	-	-	30 ± 4	25
	WQS	-	-	52 ± 11	36

[a]9–11 November 2007.
[b]12–17 November 2007.
[c]Mean ± 95% confidence interval.

Table 2. Comparison of Simulated Hourly Mean Meteorological Parameters With Observation Data[a]

Meteorological Variables	No. Stations	Mean		Δ	MAE	RMSE	COE	HR
		Sim.	Obs.					
2 m temperature (°C)	19	21.8	21.4	0.4	1.4	1.7	0.81	0.70
2 m relative humidity (%)	9	77	71.1	5.9	9.3	11.1	0.75	0.65
10 m wind direction (deg)	16	-	-	-	-	-	0.46	0.57
10 m wind speed (m s^{-1})	16	4.4	2.9	1.5	1.8	2.1	0.53	0.32

[a]Abbreviations are as follows: Δ, difference; COE, correlation coefficient; HR, hit rate MAE, mean absolute error; RMSE, root mean square error.

3.1.3. NMHC Ratios and Their Relationship With Ozone

[16] VOC samples were simultaneously taken at both sites on 4 days during Period 2 (13, 15–17 November). These samples provide a means to further understand the causes of the O_3 episode event. The *m*, *p*-xylene/ethylbenzene ratio is one of the most widely used VOC ratios for identifying the photochemical age of air masses [e.g., *So and Wang*, 2004; *Guo et al.*, 2007]. Since *m*- and *p*-xylene are more photochemically reactive than ethylbenzene, the ratio decreases with the progress of photochemical reactions. Figure 5a shows the scatter plot of *m*, *p*-xylene versus ethylbenzene at both sites. At TC the ratio was 1.9 ± 0.26 pptv/pptv, much higher than at WQS (0.81 ± 0.15 pptv/pptv), indicating that the air masses arriving at TC were more fresh than those arriving at WQS. Compared to the *m*, *p*-xylene/ethylbenzene ratio found during the entire sampling period (October–November 2007) at TC and WQS (1.07 ± 0.07 and 0.91 ± 0.07 pptv/pptv, respectively), it is clear that the air masses arriving at TC during Period 2 were more fresh than other days, while air parcels arriving at WQS were more aged in Period 2 than other days for the whole sampling period. Therefore, in addition to having lower precursor concentrations (see section 3.1.2), the TC Period 2 air masses had less time for the photochemical creation of ozone. Indeed, a strong negative correlation between O_3 and the *m*, *p*-xylene/ethylbenzene ratio was found at WQS (Figure 5b). Namely, low *m*, *p*-xyleneethylbenzene ratios corresponded to high O_3 levels, and vice versa. In other words, as the air mass aged (lower ratios), secondary reactions occurred and the accumulated O_3 production increased. In contrast, a very weak correlation was found at TC. The results imply that strong photochemical O_3 formation occurred at WQS in Period 2, whereas the photochemical reactions at TC were weak.

3.2. Synoptic Weather Conditions During the Episode Event

3.2.1. Hourly Surface Meteorological Factors

[17] Many studies have shown that weather conditions play an important role in the formation of photochemical smog [e.g., *Wang et al.*, 2003; *Wang et al.*, 2006]. Figure 6 shows the temporal variations of the main meteorological factors (temperature, relative humidity, solar radiation, and wind) measured at the two sites during the period 8–17 November. Both temperature and solar radiation at the two sites increased markedly on 9 November in comparison with 8 November, in correspondence with the enhanced O_3 levels on 9 November. At WQS, relatively high temperatures were found from 9 to 17 November (maximum of about 27°C), which were favorable to the formation of photochemical smog. However, the daily maximum temperatures at TC were generally about 2°C lower than those at WQS during the entire episode event (except on 9 November). The wind field was another meteorological factor with an obvious discrepancy between the two sites. During Period 1, the wind at WQS was strong and generally northeasterly, and the wind at TC was northerly during the daytime, resulting in strong regional transport from the inland PRD region. On the other hand, during Period 2,

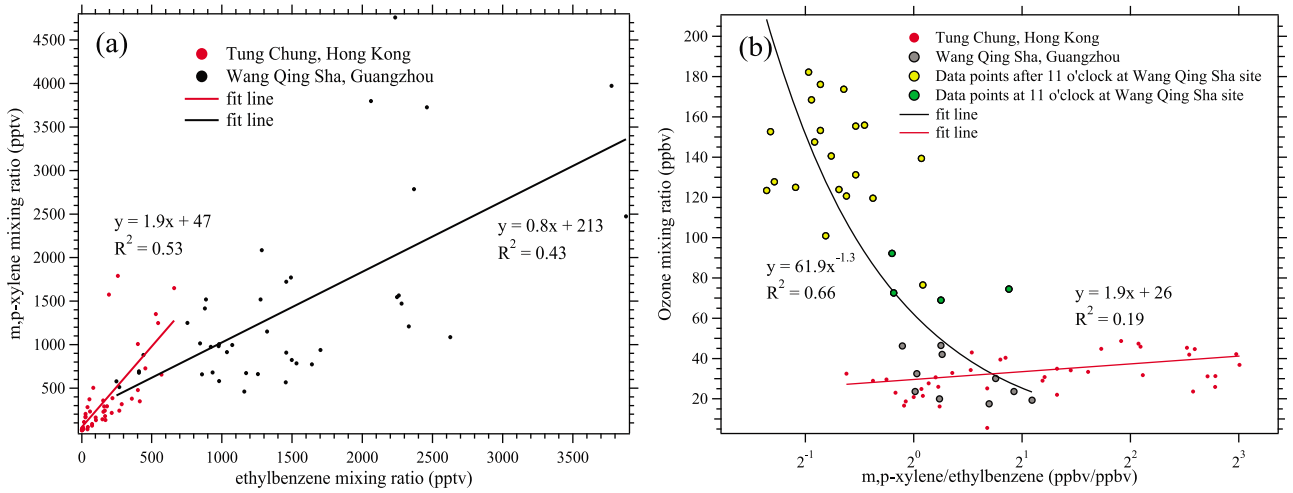

Figure 5. (a) Scatter plots of *m*/*p*-xylene with ethylbenzene and (b)their ratio with O_3 at TC and WQS sites during 4 VOC sampling days (13, 15–17 November 2007).

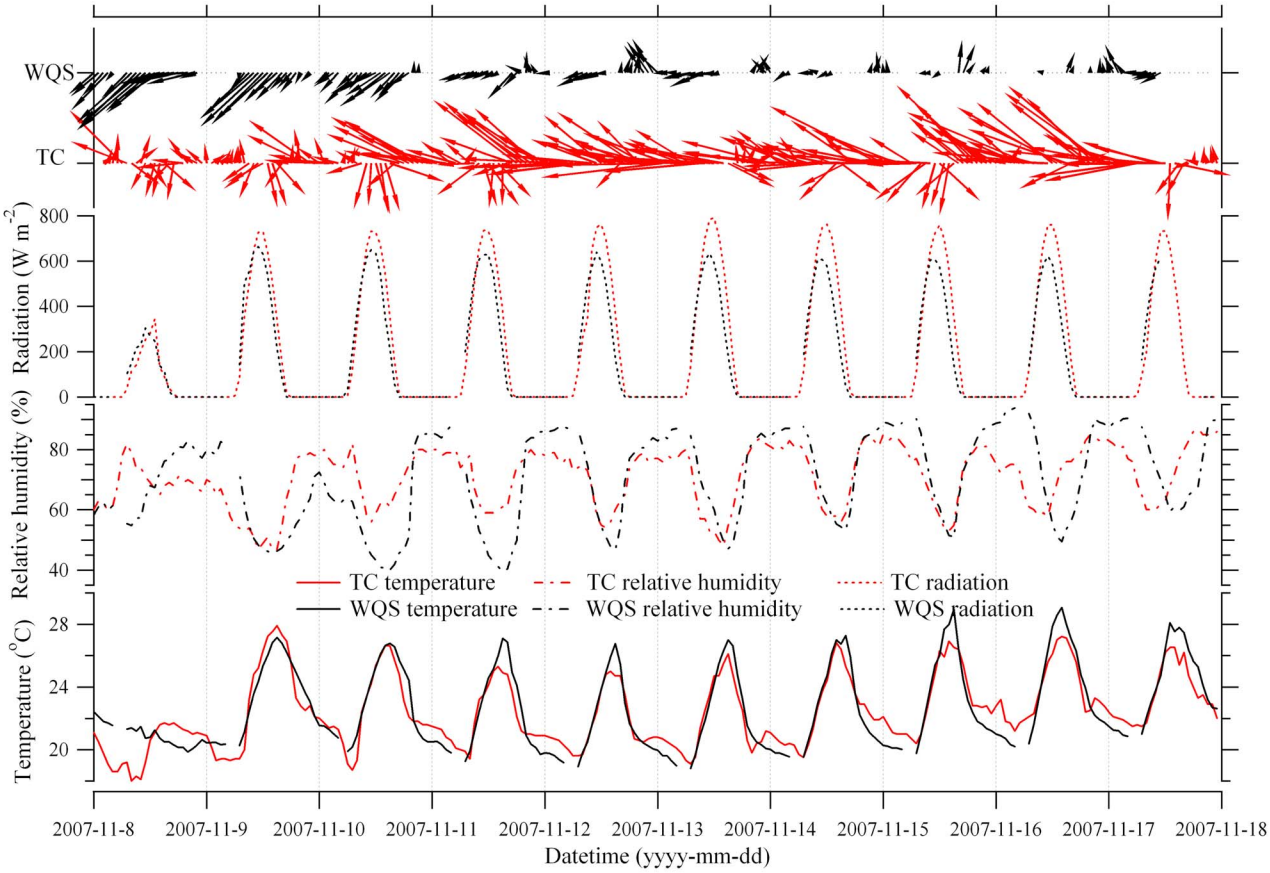

Figure 6. Temporal variations of meteorological factors at TC and WQS between 0000 LST 8 November and 2300 LST 17 November 2007.

the wind speed at WQS became weak (<1.0 m s^{-1}). Obvious sea-land breezes were observed, with a slight northerly wind during the daytime and southerly wind at nighttime. These meteorological conditions suggest that the boundary layer at WQS was stable. In contrast, strong easterly/southeasterly winds were measured at the TC site during Period 2, with wind speeds even higher than in Period 1. The easterly and southeasterly winds brought clean air masses from the South China Sea to the TC site and diluted the air pollution over the Hong Kong area. The different patterns of temperature and wind between the two sites are likely the main reasons for the O_3 patterns. In addition, atmospheric stability could be another cause of different O_3 pollution between the two sites. This issue will be discussed in the following section.

3.2.2. Weather Conditions and Vertical Profiles

[18] Hong Kong and Guangzhou had similar weather conditions on 10 November: both were at the southern edge of a high-pressure system that was located in northern China (Figure 7a). Generally, the O_3 episodes in Hong Kong are related to three typical weather systems: tropical cyclones, continental anticyclones, and low-pressure troughs [*Chan and Chan*, 2000; *Huang et al.*, 2005, 2006]. In this study, the O_3 episode in Hong Kong in Period 1 occurred under the control of a continental anticyclone, which was associated with the winter monsoon and would bring continental outflow to Hong Kong. A previous study [*Chan and Chan*, 2000] showed that a continental anticyclone was the most important contributor to the O_3 episodes observed in Hong Kong and that, commonly, the long-range transport of O_3 and other air pollutants from upwind distant sources in the East Asian region was the main reason for the high O_3 mixing ratio. However, on 15 November a relatively weak high-pressure system was present over southern China. Guangzhou was located near the center of the high-pressure system and was fully controlled by it, while Hong Kong was located at the edge of the system (Figure 7b). This pattern is consistent with the meteorological conditions usually observed in the autumn when the air mass movements from both the North China and South China Sea are weak, which leads to a fairly stable weather system. Such a stable system usually results in severe photochemical pollution in the PRD region. This weak high-pressure system remained in place from 12 to 17 November, very likely leading to different air masses being received at the two sites.

[19] The atmospheric thermal stability and vertical wind profile could also have a significant impact on the diffusion of air pollutants near the surface [e.g., *Wang and Kwok*, 2003]. Therefore, we investigated the vertical profiles of temperatures, relative humidity, and wind fields in Guangzhou and Hong Kong at 0800 LST on 10 and 15 November (Figure 8). The vertical profile data for Hong Kong were obtained from the King's Park station (45004, 22.32°N,

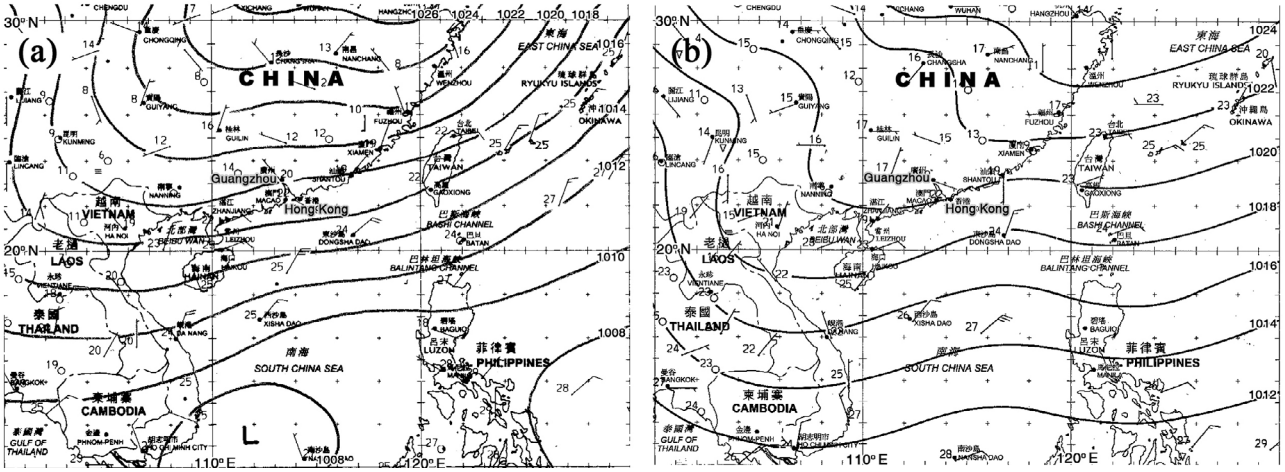

Figure 7. Surface weather charts at 0800 LST on (a) 10 November and (b) 15 November 2007.

114.17°E), and data for Guangzhou were taken from the Qingyuan station (59280, 23.67°N, 113.05°E). Their locations can be found in Figure 2. Though the King's Park station in Hong Kong is closer to WQS than the Qingyuan station is, the vertical profile data obtained from King's Park is more representative of the meteorological conditions for Hong Kong, whereas the vertical profile data gained from the Qingyuan station is more correlated with the meteorological conditions for the inland PRD region. In fact, though the Qingyuan station is around 100 km away from WQS, weather conditions at the two sites were similar (see Figure 7). These sounding data were downloaded from the Department of Atmospheric Science, College of Engineering, University of Wyoming (http://weather.uwyo.edu/upperair/sounding.html). On 10 November, similar vertical profiles of temperatures and wind fields were found in Hong Kong and Guangzhou, indicating that they were controlled by the same air masses. Northerly winds prevailed in the lower atmosphere (pressure > 925 hPa) in both Hong Kong and Guangzhou, but the wind speeds were much lower in Hong Kong (4.2 ± 1.4 m s^{-1}, compared to 8.0 ± 3.1 m s^{-1} in Guangzhou), probably because of the influence of complex topography in northern Hong Kong. The prevailing northerly winds with higher speeds in Guangzhou may also indicate the potential transport of air pollution from the inland PRD region. In contrast, on 15 November the vertical profiles in Hong Kong were entirely different from those in Guangzhou. An obvious isothermal layer with slower wind speeds (<5 m s^{-1}) was observed in the lower atmosphere of Guangzhou, coupled with a slight temperature inversion in the lowest atmosphere that would suppress mixing and would be favorable to the formation of photochemical smog. However, in Hong Kong the prevailing winds were much stronger, and wind directions were more easterly.

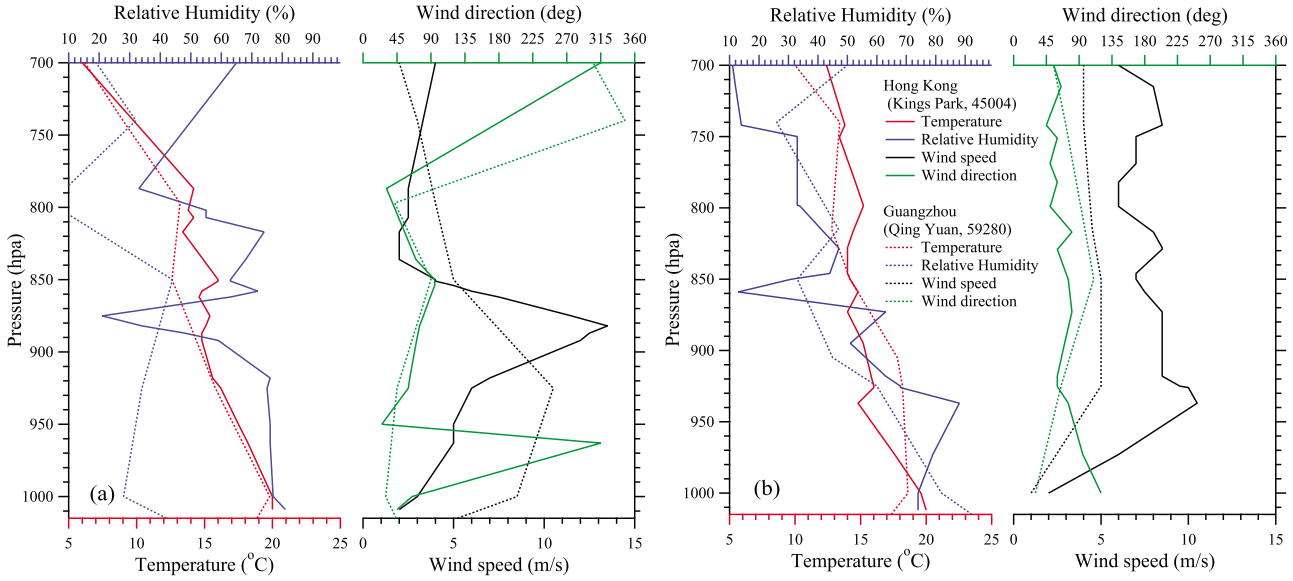

Figure 8. Atmospheric vertical structures at 0800 LST on (a) 10 November and (b) 15 November 2007.

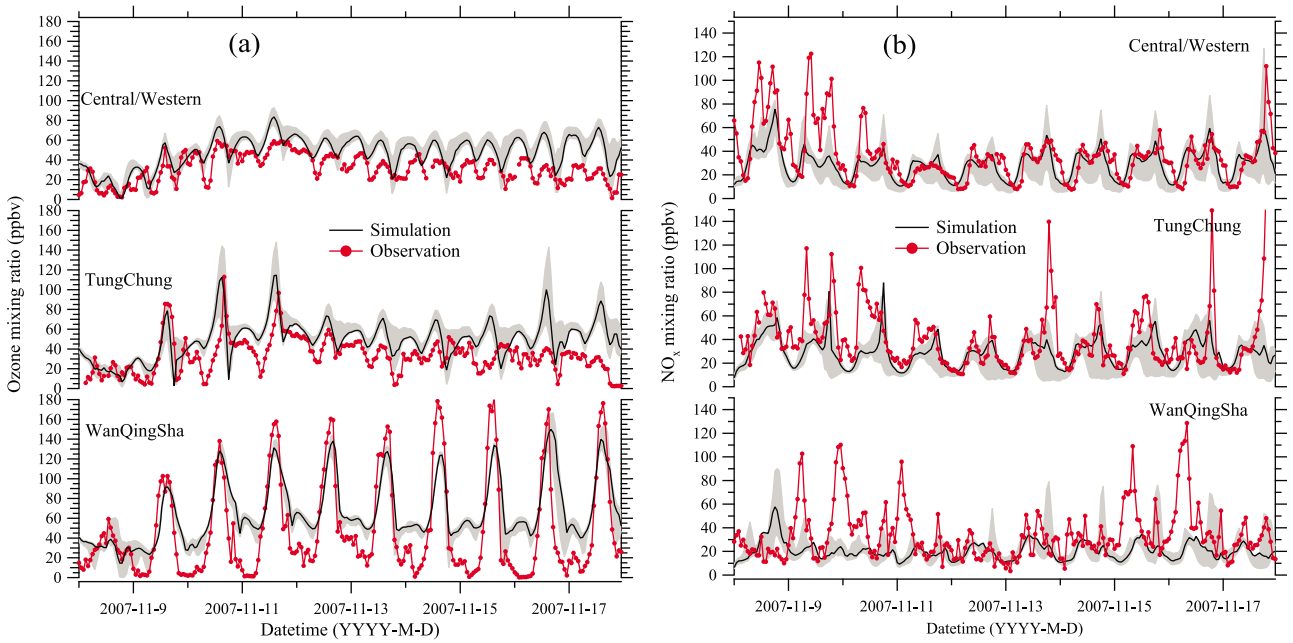

Figure 9. Time series of (a) O_3 and (b) NO_x measured at WQS, TC, and CW sites for the study period as compared to the simulation results of domain DM3 (red line with mark: observations; black line: simulations; gray shade: the mixing ratio range surrounding the corresponding model grid of the observation sites).

Moreover, no temperature inversion layer or isothermal layer was found, suggesting that vertical transport or diffusion of air pollutants could occur with ease. It is noteworthy that the vertical profiles of temperature in the lower atmosphere of Hong Kong on these two days (10 and 15 November) were somewhat similar, but the wind directions were different, which further proved that different air masses arrived in Hong Kong on these two days. That is, the air quality in Hong Kong on 10 November was predominantly affected by the inland PRD region, whereas the air quality on 15 November was mainly controlled by Hong Kong local pollution superimposed on cleaner marine air masses brought in by the easterly winds. This interpretation is consistent with the particle release simulation results presented in *Guo et al.* [2009] and with the lower CO levels that were measured at TC during Period 2.

3.3. Model Validation and Performance

[20] It is well known that field measurement data can be used to validate the simulation results of meteorological models such as the WRF and CMAQ modeling systems. In this study hourly mean 2 m temperature (T2), 2 m relative humidity (RH2), 10 m wind direction (WD10) and 10 m wind speed (WS10) at 19 meteorological observation stations were compared with simulations for domain DM3 from 0000 LST 08 November to 2300 LST 17 November, 2007. Of the observation stations, 9 are located in Hong Kong and 10 are distributed throughout the inland PRD region. The hit rate, the root mean square error, the correlation coefficient, and other statistical parameters were calculated for each station (Table 2). Overall, the simulated T2, RH2, and WS10 were all slightly higher than the observed data, with mean differences of 0.4°C, 5.9%, and 1.5 m s^{-1}, respectively. The respective correlation coefficients of T2 and RH2 were 0.85 and 0.75, reflecting good agreement between the observation data and simulation results. Nevertheless, the 10 m wind did not match well, with a correlation coefficient of 0.46 and 0.53 for WD10 and WS10, respectively. The hit rate refers to the fraction of the total records that were within a certain threshold, which is a reliable measure for evaluating model performance, as it considers the measurement uncertainty [*Schlünzen and Katzfey*, 2003]. The criteria for an acceptable hit rate calculation are that the agreement between simulation and observation data must be within 2°C for T2, 10% for RH2, 30° for WD10, and 1 m s^{-1} for WS10. On the basis of these thresholds, the hit rates of T2, RH2, and WD10 in this study were calculated to be 0.70, 0.65, and 0.57, respectively, indicating that the model basically reproduced the variation patterns of temperature and humidity as well as the trend of wind direction. However, the hit rate of WS10 (0.32) was lower in comparison with that of other variables. Considering the fact that the mean observed 10 m wind speed was 2.9 m s^{-1}, the criteria for the hit rate calculation of wind speed (1 m s^{-1}) was actually rather strict. Additionally, the wind field is a result of many complicated physical processes and is usually characterized by considerable small-scale variability, which makes it much more difficult than other parameters to simulate accurately. In general, the statistical results suggest that the WRF modeling system reasonably matched the observation data for the episode event.

[21] We further evaluated the performance of the WRF model by comparing the simulation results with the measurement data of O_3 and NO_x collected at three stations (WQS, TC, and CW). Figure 9 shows the comparison of the modeled and observed hourly mixing ratios at the three sites during the study period. The correlation coefficients at the WQS, TC, and CW sites were 0.82, 0.55, and 0.67,

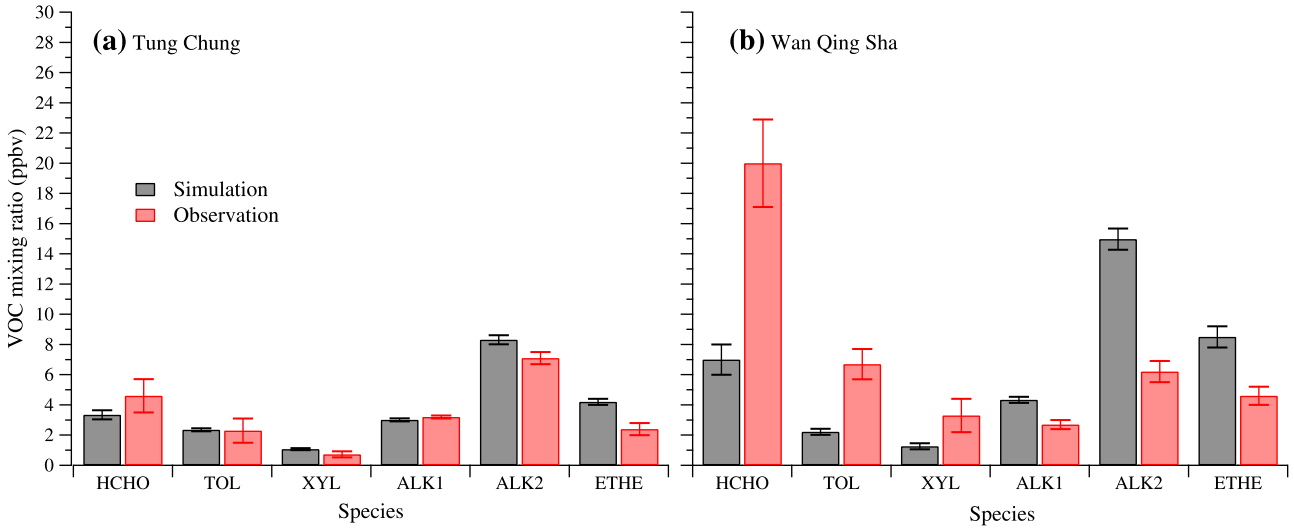

Figure 10. Comparison of the mean mixing ratios of six selected VOC species between the model simulation for domain DM3 and the observation data at (a) TC and (b) WQS (HCHO: formaldehyde; TOL: primarily toluene and other monoalkyl benzenes; XYL: primarily xylenes and polyalkyl benzenes; ALK1: ethane; ALK2: propane and acetylene; ETH; ethene).

respectively. The model reproduced well the continuous high O_3 pollution trend during this episode event at WQS. However, the daily O_3 peaks at WQS were underestimated by about 15%, and the levels at nighttime were overpredicted, due in part to NO_x mixing ratios being highly underestimated at nighttime. On the other hand, the model accurately captured the elevated O_3 mixing ratios in Period 1 (9–11 November) and the sustained low O_3 levels throughout Period 2 (12–17 November) at the TC and CW sites. In addition, the O_3 values in Hong Kong during Period 2 were overestimated, partly because the O_3 mixing ratios over the marine atmosphere of the South China Sea were overestimated, as the emissions from ships over the ocean were not considered in the inventories developed by *Zhang Q. et al.* [2009]. Furthermore, the errors generated in wind simulation might be another reason for the difference between modeled and observed air pollutants.

[22] On most of the days during the episode event, the modeled NO_x showed good agreement with the measurements at CW. However, the NO_x mixing ratios were often underestimated at WQS and TC, and at CW during the high O_3 days (9–10 November). In particular, the model did not reproduce the NO_x peaks efficiently on some days. The mean differences between modeled and measured NO_x at WQS, TC, and CW were −14.0, −12.6 and −7.5 ppbv, respectively. Since NO_x mixing ratios are generally influenced by local emissions, such as vehicular exhaust, it is relatively difficult for the model to simulate them well. Moreover, the elevated NO_x mixing ratios at WQS on some days might relate to the chimney emissions of an upwind power plant, which were not well characterized by the model.

[23] Because ambient VOCs were measured at TC and WQS on 4 days of Period 2, the results simulated by the WRF model for domain DM3 were validated with the measurement data. Six organic species used in the SAPRC-99 mechanism were selected for comparison (see Figure 10), as they are the major VOCs species in the atmosphere of the PRD region. Figure 10 compares the mean mixing ratios of these six species between the model simulation and the observation data at both sites. The modeled VOC levels at TC were close to the observed values. However, the VOC mixing ratios at WQS were poorly simulated. In particular, the levels of formaldehyde and aromatics were significantly underestimated, whereas alkanes and ethene were overestimated. The poor simulation of VOCs at WQS might be due to the fact that the VOC sources in the inland PRD region were very complex, which led to high uncertainty in emission inventories in this region [*Zheng et al.*, 2009a, 2009b]. In addition, the exclusion of biomass burning from the emission inventories might be another reason for the poor simulation of VOCs at WQS, as some studies found that biomass burning in the inland PRD could be significant [*Guo et al.*, 2006; *Q. Wang et al.*, 2007; *Yuan et al.*, 2010], though other studies did not [*Bo et al.*, 2008; *Zheng et al.*, 2009b]. The quantitative influence of biomass burning on the modeling results will be specifically studied in the future.

3.4. Surface Ozone Distributions and Flow Structures

[24] After the simulation of the wind field and air pollutants using the WRF model, we further investigated the horizontal O_3 distributions at ground level. The O_3 distribution patterns in Period 1 were clearly different from those in Period 2 (Figure 11). Figures 11a and 11b illustrate the surface O_3 mixing ratios in domain DM2 and the wind fields at 1400 LST on 10 and 15 November, respectively, representing two different distribution patterns. On 10 November, the high O_3 pollution area (>90 ppbv) was located over the south part of Guangdong and Guangxi provinces. High O_3 values were also found over east China. Provinces in south China and on the east China coast were mainly dominated by strong northeast winds, which drove air masses from the east China coast to south China, and from the east part of the inland PRD to Hong Kong (Figure 12a). Figure 12a shows more detailed surface O_3 distributions and

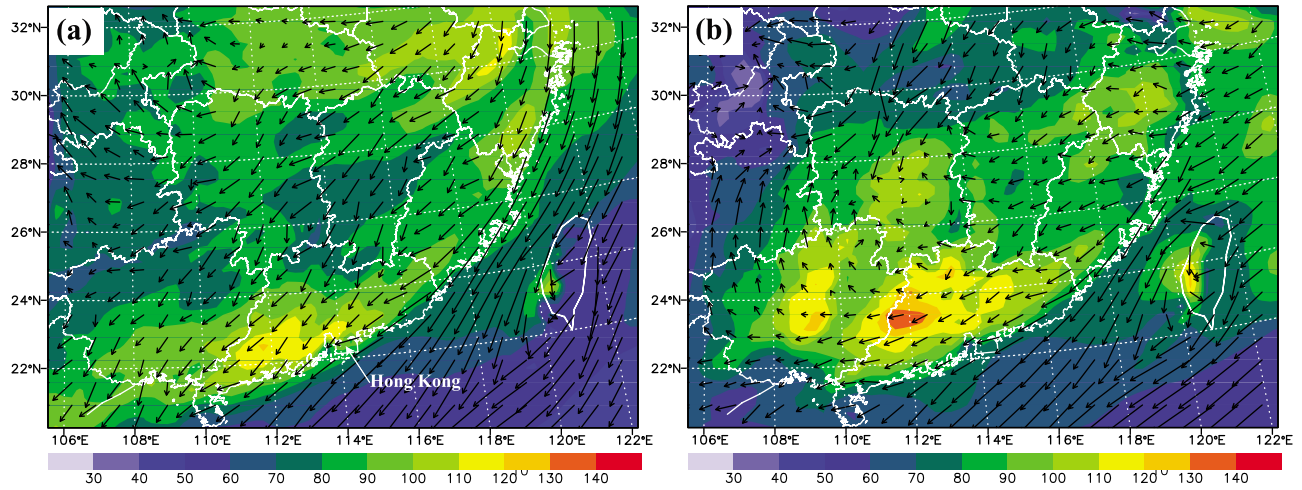

Figure 11. The distribution of simulated surface O_3 mixing ratios (shaded, ppbv) and 10 m wind (vector, m s^{-1}) in DM2 at 1400 LST on (a) 10 November and (b) 15 November 2007.

wind fields in the PRD region in the finest domain (DM3) for 4 consecutive hours on 10 November. It is clearly seen that air masses with high O_3 mixing ratios were transported from the northeast to the southwest within the inland PRD region, and the edge of the O_3-rich air masses skimmed over the Hong Kong area, explaining the high O_3 values measured at this time.

[25] As mentioned in section 3.2.2, on 15 November, a weak high pressure system was formed over Guangdong, Guangxi, Hunan, and Jiangxi provinces, corresponding to an anticyclone flow structure over the region (Figure 12b). The prevailing wind direction was easterly in Guangdong province of south China. Because of the influence of this weather system, a high O_3 area (>90 ppbv) was found in Guangdong, Guangxi, and Hunan provinces, with the highest O_3 levels in the downwind PRD region, i.e., the western part of Guangdong province. Hong Kong was also dominated by easterly wind, which brought clean air masses from the ocean to Hong Kong, causing low O_3 levels in Period 2 (Figure 12b). The different flow patterns in Period 1 and 2 are consistent with the weather conditions discussed in section 3.2.

[26] *Wang et al.* [2010] identified three O_3 distribution patterns in the PRD region in October 2004: "O_3-south," "O_3-southwest," and "O_3-west" patterns. In this study, the O_3 distribution in Period 1 was somewhat similar to the "O_3-south" pattern, while it was the same as "O_3-west" pattern in Period 2. It is noteworthy that the O_3 levels in the Hong Kong urban area were lower than in the surrounding areas for both periods (see Figures 12a and 12b), probably because of titration by high NO_x emissions. This behavior is consistent with the analysis of O_3 data at different Hong Kong sites, as discussed in section 3.1.1.

3.5. Analysis of the Mechanism of O_3 Formation

[27] To understand the mechanism of O_3 formation during this event, the contributions of individual physical and chemical processes to ground-level O_3 mixing ratios have been calculated by the process analysis module during CMAQ simulation. Table 3 shows the contributions of horizontal and vertical transport, vertical diffusion, dry deposition, and photochemical reactions to O_3 formation in the first simulated layer (0–50 m above ground level (AGL)) at the TC and WQS sites during the episode event. The contributions at each site were represented by the average values of nine grids in domain DM3 (the center one at the site with eight surrounding grids). The daily contributions were accumulated from 0800 to 1600 LST every day. The contributions on 8 November, a day that was not part of the O_3 episode, are also listed for comparison. The analysis showed significantly different patterns for physical and chemical processes at the two sites. At TC, horizontal transport and vertical diffusion were the main contributors to the O_3 increase, while at WQS photochemical production and vertical diffusion were dominant.

[28] As discussed in previous sections, at the TC site the O_3 levels produced by horizontal transport were high during Period 1, and the mean accumulated contribution of horizontal transport to the O_3 level was 261 ± 58 ppbv D^{-1} (D is defined as hours from 0800 to 1600 LST), accounting for 70% of the total contribution from all O_3 sources. However, during Period 2 at TC, the contribution of horizontal transport significantly decreased to a mean value of 145 ± 62 ppbv D^{-1}. Vertical diffusion was another important contributor to net O_3 mixing ratios. Nevertheless, no significant difference was found between the two periods, with the mean accumulated values being 112 ± 23 and 104 ± 5 ppbv D^{-1}, respectively. In contrast, the contributions of photochemistry in Period 1 and Period 2 were all negative, with the average accumulated contributions being -38 ± 14 and -54 ± 14 ppbv D^{-1}, respectively. It is well known that O_3 is not only produced but also destroyed by photochemical processes. When the photochemical loss is greater than the photochemical production, the net contribution of photochemical reactions to the O_3 formation is negative. Generally, in daytime, most O_3 is photochemically generated at noon but consumed in the morning and late afternoon (see Figure 13).

[29] To further explore O_3 formation at TC, Figures 13a and 13b illustrate the mean diurnal variations of the contributions of each process to O_3 formation in the first simulated vertical layer (0–53 m AGL) in the two periods at TC. In

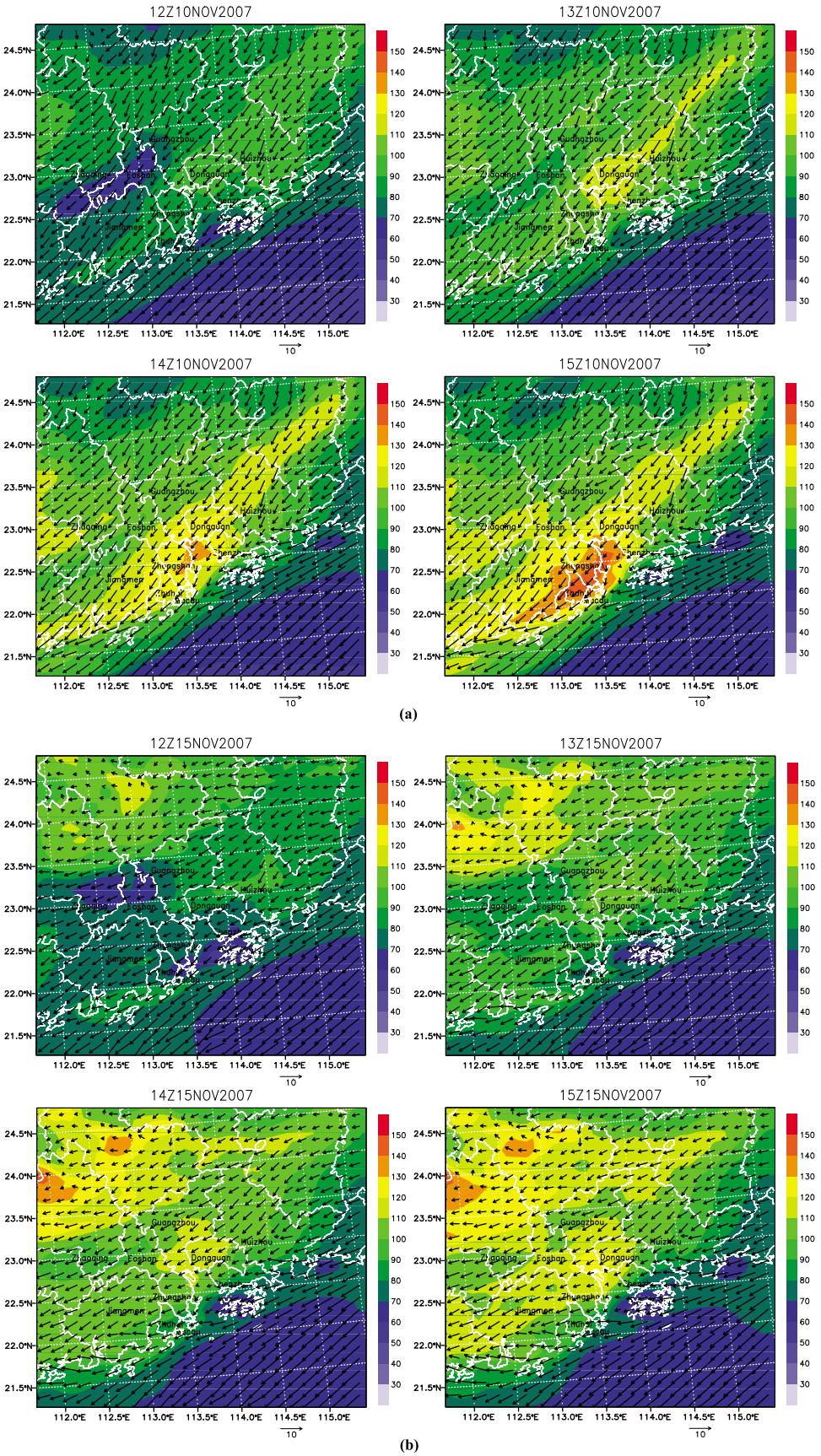

Figure 12. The distribution of surface O_3 mixing ratios (shaded, ppbv) and 10 m wind (vector, m s^{-1}) in domain DM3 for 4 consecutive hours (1200–1500 LST) on (a) 10 November and (b) 15 November 2007).

Table 3. Contributions (in ppbv D^{-1}) of Different Processes to the O_3 Formation in the First Simulated Vertical Layer (0–50 m AGL) Accumulated From 0800 to 1600 LST During the Study Period at TC and WQS[a]

	TC						WQS					
Date	hadv	vadv	vdif	ddep	chem	**net**[b]	hadv	vadv	vdif	ddep	chem	**net**[b]
08 Nov.	−69	42	112	−2	−86	**−3**	47	−45	96	−28	−63	**8**
09 Nov.	201	−177	88	−7	−52	**53**	58	−60	71	−49	24	**46**
10 Nov.	290	−310	126	−11	−30	**65**	105	−111	85	−76	70	**72**
11 Nov.	292	−310	121	−12	−31	**59**	65	−71	89	−85	68	**67**
12 Nov.	98	−127	112	−10	−59	**17**	25	−4	94	−79	52	**88**
13 Nov.	151	−176	105	−10	−45	**27**	−39	52	98	−76	44	**80**
14 Nov.	15	−32	109	−10	−77	**8**	2	18	87	−78	60	**89**
15 Nov.	190	−209	102	−10	−60	**16**	11	34	80	−80	68	**112**
16 Nov.	231	−258	94	−11	−29	**31**	55	−19	71	−83	72	**97**
17 Nov.	185	−212	104	−12	−53	**16**	13	−4	92	−91	88	**99**

[a]Abbreviations are as follows: chem, chemistry; D, hours from 0800 to 1600 LST; ddep: dry deposition; hadv, horizontal advection; TC, Tung Chung site, vadv, vertical advection; vdif, vertical diffusion; WQS, Wan Qing Sha site.
[b]net = hadv + vadv + vdif + ddep + chem.

the early morning, the O_3 mixing ratios were attributed to vertical diffusion and vertical advection, while the photochemical process and horizontal transport were favorable to the removal of O_3. At noon, with the increase in surface wind speeds (see Figure 6), the contribution of horizontal transport to the O_3 level at TC began to increase, whereas the contribution of vertical diffusion decreased because of enhanced turbulent mixing, which led to a decrease in the vertical gradient of O_3 mixing ratios. In addition, slight photochemical generation (<5 ppbv hr^{-1}) at noontime was found in both periods. The contribution of horizontal transport reached its maximum at 1600 LST in Period 1 and at 1400 LST in Period 2. The hourly peak value of the contribution of horizontal transport in Period 1 was 82 ppbv h^{-1}, twice that in Period 2 (41 ppbv h^{-1}), suggesting that the characteristics of the horizontal transport may differ between

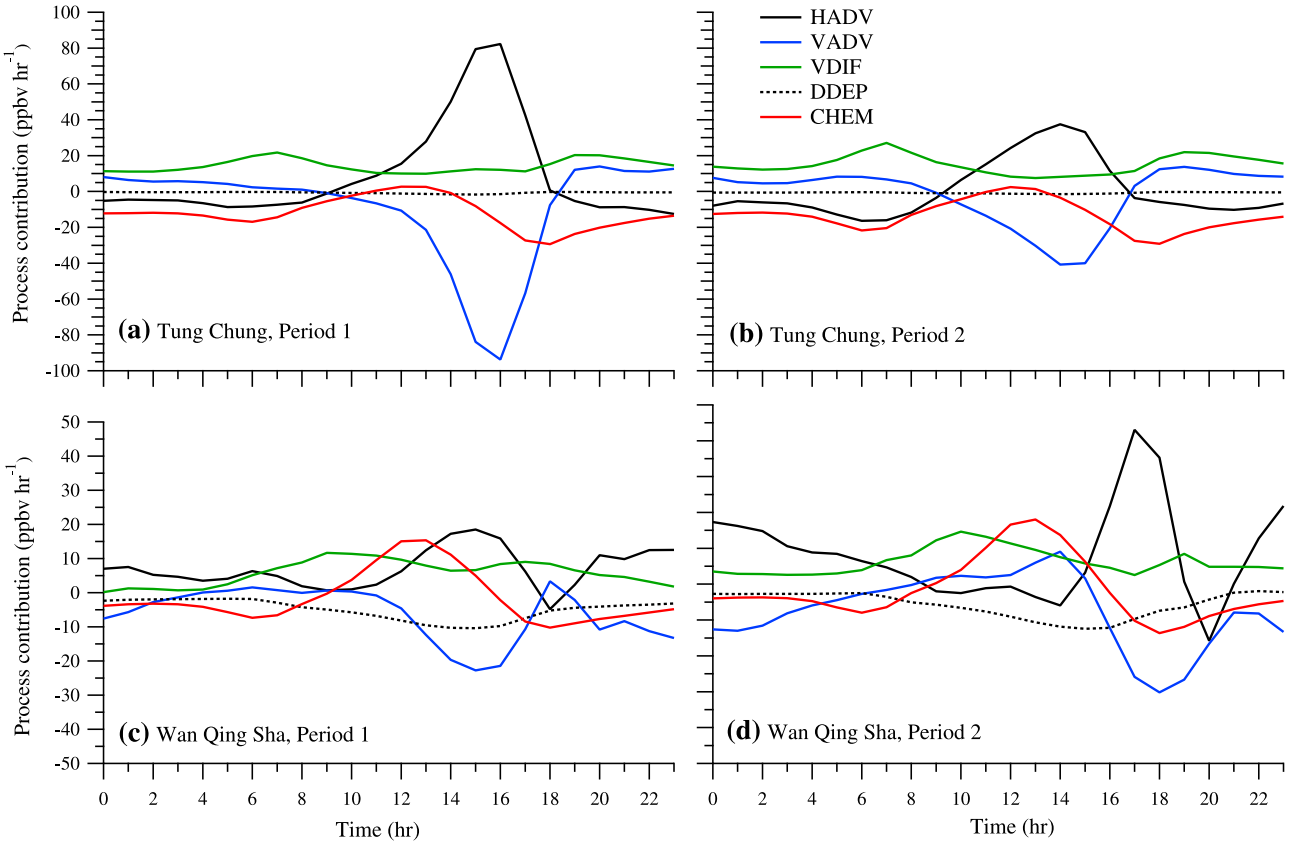

Figure 13. Mean diurnal variations of the contributions (in ppbv D^{-1}) of each process to O_3 formation in the first simulated vertical layer (0–53 m above ground level) in the two periods (a, b) at TC and (c, d) at WQS. (Abbreviations are as follows: chem, chemistry; D, hours from 0800 to 1600 LST; ddep, dry deposition; hadv, horizontal advection; vadv, vertical advection; vdif, vertical diffusion).

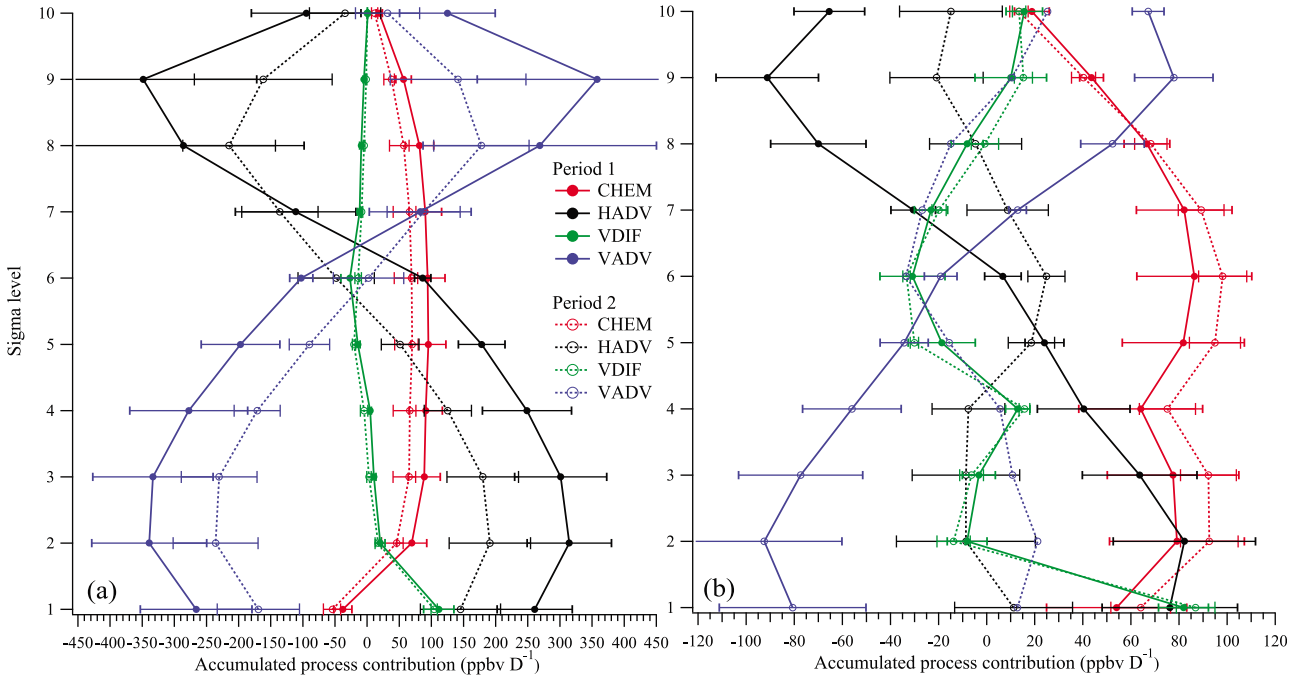

Figure 14. The mean contributions (in ppbv D^{-1}) of accumulative processes in the lowest 10 model levels (approximately 0–1500 m AGL) in the two periods at (a) TC and (b) WQS (hadv, horizontal advection; vadv, vertical advection; vdif, vertical diffusion; chem, chemistry).

the two periods. The obvious peak for horizontal transport at 1600 LST in Period 1 was consistent with the observed sharp O_3 peak at the same time (see Figure 4).

[30] The consistently positive contribution of vertical diffusion to O_3 levels at TC during the daytime indicates that the O_3 mixing ratio in the upper layers was much higher. Hence, we further examined the O_3 formation in the whole boundary layer. The mean contributions of accumulative processes in the lowest 10 model levels (approximately 0–1500 m AGL) in the two periods are shown in Figure 14a. Significantly positive contributions of horizontal transport were found in the lowest six layers (approximately 0–700 m AGL) in Period 1, with a peak value of 315 ± 65 ppbv D^{-1} in the second layer, much higher than that in Period 2 (191 ± 63 ppbv D^{-1}). Additionally, clear photochemical O_3 generation was found between the second and ninth layers (approximately 50–1200 m AGL), with a value of about 80 ppbv D^{-1} in both periods. The negative contribution of photochemical processes at ground level was related to the high NO_x emission in Hong Kong, similar to that found in the Guangzhou urban area [*Wang et al.*, 2010]. Overall, the strong horizontal transport led to the occurrence of high O_3 mixing ratios in Period 1, while the lower horizontal transport ($p < 0.05$) mainly resulted in relatively low net O_3 formation and subsequent lower O_3 mixing ratios in Period 2. The above results clearly reveal the importance of horizontal transport to O_3 formation in Hong Kong.

[31] At the WQS site, photochemical O_3 production was extremely strong, starting on 9 November (46 ppbv D^{-1}) and remaining mostly above 80 ppbv D^{-1} from 10 to 17 November. Vertical diffusion was another main contributor to the O_3 formation. The average contribution of vertical diffusion was 85 ± 6 ppbv D^{-1} at WQS during the study period. The results imply that the contributions of photochemical production and vertical diffusion were comparable at WQS during the episode. We also found that the mean contribution of horizontal transport in Period 1 was 76 ± 28 ppbv D^{-1}, comparable to the photochemical process, whereas it was only 11 ± 24 ppbv D^{-1} in Period 2. The results are consistent with the discussion in section 3.2.1. Analysis of the diurnal contributions of various physical and chemical processes to O_3 mixing ratios at WQS indicated that photochemical production mainly occurred at noontime with a peak at 1300 LST, while horizontal transport played an important role in the afternoon, with a maximum value at 1500 LST in Period 1 (see Figure 13c). Similarly, the highest values as a result of photochemical production and horizontal transport in Period 2 were observed at 1300 and 1700 LST, respectively (see Figure 13d). The high contributions of regional transport in late afternoon and at nighttime were caused by sea-land breezes, perhaps with vertical transport, which resulted in the overestimation of simulated O_3 mixing ratios at nighttime (see Figure 9a). Furthermore, in the boundary layer, the photochemical O_3 generation during the two periods was considerably high at the level below 1000 m AGL (about 80 ppbv D^{-1}). Overall, in Period 1, the processes of horizontal transport and photochemistry had comparable contributions to the O_3 mixing ratios in the lowest three layers (approximately 0–250 m AGL), whereas only photochemical production contributed to the O_3 values in Period 2 (Figure 14b).

4. Summary and Conclusions

[32] We present an interesting O_3 pollution event in the PRD region during 9–17 November 2007. The O_3 episode

(daily hourly maximum > 122 ppbv) lasted a week in Guangzhou (WQS), from 10 to 17 November, with the highest hourly O_3 level being 182 ppbv. However, even though the Hong Kong site (TC), is only 62 km away from the Guangzhou site, only one O_3 episode day (10 November) was observed in Hong Kong, and from 12 to 17 November the O_3 mixing ratios remained around 40 ppbv. The mean O_3 levels at TC and WQS were 38 ± 3 and 51 ± 7 ppbv, respectively.

[33] On the basis of different O_3 levels in Hong Kong, we divided this episode event into two periods: 9–11 November as Period 1 and 12–17 November as Period 2. In addition to O_3 itself, the mixing ratios of O_3 precursors (NO_x and CO) showed significant differences between the two periods at TC, but no obvious differences were found at WQS. The results indicate that the air masses arriving at TC in the two periods were different, while similar air masses were characterized in the two periods at WQS. Analysis of the ratio of VOC species reveals that the air masses at TC in Period 2 were much fresher than those at WQS. The relationship between O_3 and the *m*, *p*-xylene/ethylbenzene ratio suggests that strong photochemical O_3 formation took place at WQS, whereas weak photochemical reactions occurred at TC during Period 2. The prevailing wind was northerly with a relatively high wind speed at both sites during Period 1, suggesting the impact of regional transport from the inland PRD. In contrast, obvious differences in temperature and wind were found between TC and WQS during Period 2 (specifically, weaker winds and higher temperatures at WQS compared to strong easterly winds and lower temperatures at TC), which explain the difference in air pollutant concentrations to a certain extent.

[34] A comprehensive air quality model system (WRF-CMAQ) was used to simulate this O_3 pollution event. The simulated meteorological fields (T2, RH2, WS10, and WD10) of modeling domain DM3 in the PRD were compared with observations at up to 19 monitoring sites. The modeled T2, RH2, and WS10 values were all slightly higher than the observed data, with mean differences of 0.4°C, 5.9%, and 1.5 m s^{-1}. The correlation coefficients of T2, RH2, WD10, and WS10 were 0.85, 0.75, 0.46, and 0.53, respectively, indicating that the model generally reproduced the variations of weather conditions. The model system reasonably reproduced the continuous high O_3 pollution during this episode event at WQS. It also captured well the elevated O_3 mixing ratios in Period 1 and sustained low O_3 levels throughout Period 2 at TC.

[35] The modeled surface O_3 distributions and flow structures clearly illustrated the processes of regional transport of O_3 during Period 1 in the PRD region and verified the various air masses received in Hong Kong in the two periods. Process analysis of O_3 formation showed that horizontal transport and vertical diffusion were the main contributors to the O_3 increase at TC, while O_3 levels were dominated by photochemical production and vertical diffusion at WQS. The findings help to characterize the interaction of air pollution between the inland PRD region and Hong Kong. This is the first time that concurrent air quality measurements have been made in the inland PRD and Hong Kong. The observed meteorological features were characteristic for autumn in this region, and future concurrent studies can determine whether such prolonged O_3 episodes in Guangzhou compared to Hong Kong are a common occurrence in this region.

[36] **Acknowledgments.** The authors thank Steven Poon, Zhengyue Li, and Wai Chun Tse for their help with sample collection. The project is supported by the Research Grants Council of the Hong Kong Special Administrative Region (projects PolyU 5163/07E and PolyU 5179/09E), NSFC/RGC joint project (40931160436 and 3-ZG36), the Research Grant (A-PC0G) of the Hong Kong Polytechnic University, the National Key Basic Research Support Foundation of China (grant 2006CB403706, 2006CB403703), the 973 project (2010CB428503, 2006CB403706), and the 863 project (2006AA06A307) from Ministry of Science and Technology of China.

References

Barna, M., and B. Lamb (2000), Improving ozone modeling in regions of complex terrain using observational nudging in a prognostic meteorological model, *Atmos. Environ.*, *34*, 4889–4906.

Binkowski, F. S. (1999), The aerosol portion of Models-3 CMAQ, in *Science Algorithms of the EPA Models-3 Community Multiscale Air Quality (CMAQ) Modeling System*, edited by D. W. Byun and J. K. S. Ching, pp. 10-1–10-16, *Rep. EPA-600/R-99/030*, U.S. Environ. Protect. Agency, Research Triangle Park, N.C.

Bo, Y., H. Cai, and S. D. Xie (2008), Spatial and temporal variation of historical anthropogenic NMVOCs emission inventories in China, *Atmos. Chem. Phys.*, *8*, 7297–7316.

Carter, W. P. L. (2000), Documentation of the SAPRC-99 chemical mechanism for VOC reactivity assessment, *Final Rep. Calif. Air Resour. Board 92–329*, Univ. of Calif., Riverside.

Chan, C. Y., and L. Y. Chan (2000), Effect of meteorology and air pollutant transport on ozone episodes at a subtropical coastal Asian city, Hong Kong, *J. Geophys. Res.*, *105*(D16), 20,707–20,724.

Chan, L. Y., H. Y. Liu, K. S. Lam, T. Wang, S. J. Oltmans, and J. M. Harris (1998), Analysis of the seasonal behavior of tropospheric ozone at Hong Kong, *Atmos. Environ.*, *32*, 159–168.

Cheng, H. R., H. Guo, X. M. Wang, S. M. Saunders, S. H. M. Lam, F. Jiang, A. J. Ding, and T. J. Wang (2010), On the relationship between O_3 and its precursors in the Pearl River Delta: Application of an observation based model (OBM), *Environ. Sci. Pollut. Res.*, *17*, 547–560, doi:10.1007/s11356-009-0247-9.

Choi, H. J., H. W. Lee, K. H. Sung, M. J. Kim, Y. K. Kim, and W. S. Jung (2009), The impact of nudging coefficient for the initialization on the atmospheric flow field and the photochemical ozone concentration of Seoul, Korea, *Atmos. Environ.*, *43*, 4124–4136.

Ding, A. J., T. Wang, M. Zhou, T. J. Wang, and Z. K. Li (2004), Simulation of sea-land breezes associated with a multi-day episode in the Pearl River Delta of China, *Atmos. Environ.*, *38*, 6737–6750.

Gipson, G. L. (1999), Process analysis, in *Science Algorithms of the EPA Models-3 Community Multiscale Air Quality (CMAQ) Modeling System*, chap. 16, edited by D. W. Byun and J. K. S. Ching, *Rep. EPA-600/R-99/030*, U.S. Environmental Protection Agency, Research Triangle Park, N.C.

Guenther, A., et al. (2006), Estimates of global terrestrial isoprene emissions using MEGAN (Model of Emissions of Gases and Aerosols from Nature), *Atmos. Chem. Phys.*, *6*, 3181–3210.

Guo, H., T. Wang, I. J. Simpson, D. R. Blake, Y. H. Kwok, and Y. S. Li (2006), Regional and local contributions to ambient non-methane volatile organic compounds at a polluted rural/coastal site in Pearl River Delta, China, *Atmos. Environ.*, *40*, 2345–2359.

Guo, H., K. L. So, I. J. Simpson, B. Barletta, S. Meinardi, and D. R. Blake (2007), C1–C8 volatile organic compounds in the atmosphere of Hong Kong: Overview of atmospheric processing and source apportionment, *Atmos. Environ.*, *41*, 1456–1472.

Guo, H., et al. (2009), Concurrent observations of air pollutants at two sites in the Pearl River Delta and the implication of regional transport, *Atmos. Chem. Phys.*, *9*, 7343–7360.

Hong Kong Environmental Protection Department (Air Science Group) (HKEPD) (2007), *Air Quality in Hong Kong 2006*.

Huang, J.-P., J. C. H. Fung, A. K. H. Lau, and Y. Qin (2005), Numerical simulation and process analysis of typhoon-related ozone episodes in Hong Kong, *J. Geophys. Res.*, *110*, D05301, doi:10.1029/2004JD004914.

Huang, J.-P., J. C. H. Fung, and A. K. H. Lau (2006), Integrated processes analysis and systematic meteorological classification of ozone episodes in Hong Kong, *J. Geophys. Res.*, *111*, D20309, doi:10.1029/2005JD007012.

Jenkin, M. E. (2004), Analysis of sources and partitioning of oxidant in the UK—Part 1: the NOX-dependence of annual mean concentrations of nitrogen dioxide and ozone, *Atmos. Environ.*, *38*, 5117–5129.

Jiang, F., T. J. Wang, T. T. Wang, M. Xie, and H. Zhao (2008), Numerical modeling of a continuous photochemical pollution episode in Hong Kong using WRF-chem, *Atmos. Environ.*, *42*, 8717–8727.

Kusaka, H., and F. Kimura (2004), Coupling a single-layer urban canopy model with a simple atmospheric model: Impact on urban heat island simulation for an idealized case, *J. Meteorol. Soc. Jpn.*, *82*, 67–80.

Lam, K. S., T. Wang, L. Y. Chan, and H. Y. Liu (1996), Observation of surface ozone and carbon monoxide at a coastal site in Hong Kong, in *Atmospheric Ozone, Proceedings of the XVIII Quadrennial Ozone Symposium*, L'Aquila, Italy, 12–21 September, 1996, edited by P. Fabian, pp. 395–398, Ecomed Publishers, Landsberg, Germany.

Liu, Y., A. Bourgeois, T. Warner, S. Swerdlin, and J. Hacker (2005), An implementation of obs-nudging-based FDDA into WRF for supporting ATEC test operations, paper 10.7 presented at 2005 WRF User Workshop, June 27–30, 2005, National Center for Atmospheric Research, Boulder, Col.

Schlünzen, K. H., and J. J. Katzfey (2003), Relevance of sub-grid-scale land-use effects for mesoscale model, *Tellus, Ser. A*, *55*, 232–246.

Shao, M., Y. H. Zhang, L. M. Zeng, X. Y. Tang, J. Zhang, L. J. Zhong, and B. G. Wang (2009), Ground-level ozone in the Pearl River Delta and the roles of VOC and NOx in its production, *J. Environ. Manage.*, *90*, 512–518.

Skamarock, W. C., J. B. Klemp, J. Dudhia, D. O. Gill, D. M. Barker, W. Wang, and J. G. Powers (2008), A description of the Advanced Research WRF Version 3, *NCAR Tech. Note NCAR/TN-475+STR*, Natl. Cent. Atmos. Res., Boulder, Colo.

So, K. L., and T. Wang (2003), On the local and regional influence on ground-level ozone concentrations in Hong Kong, *Environ. Pollut.*, *123*, 307–317.

So, K. L., and T. Wang (2004), C3–C12 non-methane hydrocarbons in subtropical Hong Kong: Spatial-temporal variations, source-receptor relationships and photochemical reactivity, *Sci. Total Environ.*, *328*(1–3), 161–174.

Stauffer, D. R., and N. L. Seaman (1990), Use of four-dimensional data assimilation in a limited-area mesoscale model, Part I: Experiments with synoptic-scale data, *Mon. Weather Rev.*, *118*, 1250–1277.

Streets, D. G., C. Yu, M. H. Bergin, X. Wang, and G. R. Carmichael (2006), Modeling study of air pollution due to the manufacture of export goods in China's Pearl River Delta, *Environ. Sci. Technol.*, *40*, 2099–2107.

Wang, Q. Q., M. Shao, Y. Liu, K. William, G. Paul, X. H. Li, Y. Liu, and S. H. Lu (2007), Impact of biomass burning on urban air quality estimated by organic tracers: Guangzhou and Beijing as cases, *Atmos. Environ.*, *41*, 8380–8390.

Wang, T., and J. Y. H. Kwok (2003), Measurement and analysis of a multi-day photochemical smog episode in the Pearl River Delta of China, *J. Appl. Meteorol.*, *42*, 404–416.

Wang, T., K. S. Lam, A. S. Y. Lee, S. W. Pang, and W. S. Tsui (1998), Meteorological and chemical characteristics of the photochemical ozone episodes observed at Cape D'Aguilar in Hong Kong, *J. Appl. Meteorol.*, *37*, 1167–1177.

Wang, T., C. N. Poon, Y. H. Kwok, and Y. S. Li (2003), Characterizing the temporal variability and emission pattern of pollution plumes in the Pearl River Delta of China, *Atmos. Environ.*, *37*, 3539–3550.

Wang, T., X. L. Wei, A. J. Ding, C. N. Poon, K. S. Lam, Y. S. Li, L. Y. Chan, and M. Anson (2009), Increasing surface ozone concentrations in the background atmosphere of Southern China, 1994–2007, *Atmos. Chem. Phys.*, *9*, 6217–6227.

Wang, T. J., K. S. Lam, M. Xie, X. M. Wang, G. Carmichael, and Y. S. Li (2006), Integrated studies of a photochemical smog episode in Hong Kong and regional transport in the Pearl River Delta of China, *Tellus Ser. B*, *58*, 31–40.

Wang, X., Y. Zhang, Y. Hu, W. Zhou, K. Lu, L. Zhong, L. Zeng, M. Shao, M. Hu, and A. G. Russell (2010), Process analysis and sensitivity study of regional ozone formation over the Pearl River Delta, China, during the PRIDE-PRD2004 campaign using the Community Multiscale Air Quality modeling system, *Atmos. Chem. Phys.*, *10*, 4423–2237.

Wang, X. M., W. S. Lin, L. M. Yang, R. R. Deng, and H. Lin (2007), A numerical study of influences of urban land-use change on ozone distribution over the Pearl River Delta region, China, *Tellus, Ser. B*, *59*, 633–641.

Yuan, B., Y. Liu, M. Shao, S. H. Lu, and D. G. Streets (2010), Biomass burning contributions to ambient VOCs species at a receptor site in the Pearl River Delta (PRD), China, *Environ. Sci. Technol.*, *44*, 4577–4582.

Zhang, J., T. Wang, W. L. Chameides, C. Cardelino, J. Kwok, D. R. Blake, A. J. Ding, and K. L. So (2007), Ozone production and hydrocarbon reactivity in Hong Kong, Southern China, *Atmos. Chem. Phys.*, *7*, 557–573.

Zhang, Q., et al. (2009), Asian emissions in 2006 for the NASA INTEX-B mission, *Atmos. Chem. Phys.*, *9*, 5131–5153.

Zhang, Y. H., S. Xie, L. Zeng, and H. Wang (1999), The traffic emission and its impact on air quality in Guangzhou area, *J. Environ. Sci.*, *11*, 355–360.

Zhang, Y. H., M. Hu, L. J. Zhong, A. Wiedensohler, S. Liu, M. Andreae, W. Wang, and S. J. Fan (2008a), Regional integrated experiments of air quality over Pearl River Delta 2004: Overview, *Atmos. Environ.*, *42*, 6157–6173.

Zhang, Y. H., et al. (2008b), Regional ozone pollution and observation-based approach for analyzing ozone-precursor relationship during the PRIDE-PRD2004 campaign, *Atmos. Environ.*, *42*, 6203–6218.

Zheng, J. Y., L. J. Zhang, W. W. Che, Z. Y. Zheng, and S. S. Yin (2009a), A highly resolved temporal and spatial air pollutant emission inventory for the Pearl River Delta region, China and its uncertainty assessment, *Atmos. Environ.*, *43*, 5112–5122.

Zheng, J. Y., M. Shao, W. W. Che, L. J. Zhang, L. J. Zhong, Y. H. Zhang, and D. G. Streets (2009b), Speciated VOC emission inventory and spatial patterns of ozone formation potential in the Pearl River Delta, China, *Environ. Sci. Technol.*, *43*, 8580–8586. doi:10.1021/es901688e.

Zheng, J. Y., L. J. Zhong, T. Wang, P. K. K. Louie, and Z. C. Li (2010), Ground-level ozone in the Pearl River Delta region: Analysis of data from a recently established regional air quality monitoring network, *Atmos. Environ.*, *44*, 814–823.

D. R. Blake and I. J. Simpson, Department of Chemistry, University of California at Irvine, CA, USA.

H. R. Cheng, H. Guo, and F. Jiang, Air Quality Studies, Department of Civil and Structural Engineering, the Hong Kong Polytechnic University, Hong Kong. (ceguohai@polyu.edu.hk)

A. J. Ding and T. J. Wang, School of Atmospheric Sciences, Nanjing University, Nanjing, China.

S. H. M. Lam and S. M. Saunders, School of Biomedical, Biomolecular, and Chemical Sciences, University of Western Australia, Perth, Australia.

X. M. Wang, Guangzhou Institute of Geochemistry, Chinese Academy of Sciences, Guangzhou, China.